A sulfonyl fluoride derivative inhibits EGFR L858R/T790M/C797S by covalent modification of the catalytic lysine

A Sulfonyl Fluoride Derivative Inhibits EGFR$^{L858R/T790M/C797S}$ by Covalent Modification of the Catalytic Lysine

*Francesca Ferlenghi,[1] Laura Scalvini,[1] Federica Vacondio,[1] Riccardo Castelli,[1] Nicole Bozza,[1] Giuseppe Marseglia,[1] Silvia Rivara,[1] Alessio Lodola,[*1] Silvia La Monica,[2] Roberta Minari,[3] Pier Giorgio Petronini,[2] Roberta Alfieri,[2] Marcello Tiseo,[2,3] and Marco Mor[1]*

[1]Department of Food and Drug, University of Parma, Parma, Italy; [2]Department of Medicine and Surgery, University of Parma, Parma, Italy; [3]Medical Oncology, University Hospital of Parma, Parma, Italy

***Corresponding Author**

Prof. Alessio Lodola,

Department of Food and Drug, University of Parma, Parma, Italy

E-mail: alessio.lodola@unipr.it

ABSTRACT

The emergence of the C797S mutation in EGFR is a frequent mechanism of resistance to osimertinib in the treatment of non-small cell lung cancer (NSCLC). In the present work, we report the design, synthesis and biochemical characterization of UPR1444 (compound **11**), a new sulfonyl fluoride derivative which potently and irreversibly inhibits $EGFR^{L858R/T790M/C797S}$ through the formation of a sulfonamide bond with the catalytic residue Lys745. Enzymatic assays show that compound **11** displayed an inhibitory activity on $EGFR^{WT}$ comparable to that of osimertinib, and it resulted more selective than the sulfonyl fluoride probe XO44, recently reported to inhibit a significant part of the kinome. Neither compound **11** nor XO44 inhibited $EGFR^{del19/T790M/C797S}$ triple mutant. When tested in Ba/F3 cells expressing $EGFR^{L858R/T790M/C797S}$, compound **11** resulted significantly more potent than osimertinib at inhibiting both EGFR autophosphorylation and proliferation, even if the inhibition of EGFR autophosphorylation by compound **11** in Ba/F3 cells was not long lasting.

KEYWORDS

EGFR; C797S; sulfonyl fluoride; lysine; covalent inhibitor; HRMS; osimertinib

Abbreviations

EGFR, epidermal growth factor receptor; NSCLC, non-small cell lung cancers; TKI, tyrosine kinase inhibitor; ATP, adenosine triphosphate; WT, wild type; TR-FRET, time-resolved fluorescence resonance energy transfer; HRMS, high-resolution mass spectrometry.

1. INTRODUCTION

The epidermal growth factor receptor (EGFR) is a tyrosine kinase receptor that transduces proliferation signals [1]. Activating mutations in the EGFR gene concur to the insurgence of non-small cell lung cancer (NSCLC). The two most frequent EGFR alterations found in NSCLC occur at the intracellular kinase domain and are represented by deletion of five exon-19 residues (E746-A750), that occurs immediately before the αC-helix, and exon-21 replacement of an arginine for leucine (L858R) in the activation segment [2] These structural alterations cause ligand-independent EGFR activation promoting tumor insurgence and progression in NSCLC patients [3]. Deletion 19 (del19) and L858R mutation also sensitize NSCLC to the treatment with EGFR tyrosine kinase inhibitors (TKIs) [4]. NSCLC patients with activating mutations respond to first generation EGFR inhibitors gefitinib (**1**) and erlotinib (Fig. 1) until resistance emerges [5]. The most frequent mechanism of resistance to gefitinib and erlotinib is the acquisition of the gatekeeper mutation T790M [6], which hampers the effect of these TKIs [7]. Development of second-generation TKI irreversible agents [8] containing a Michael acceptor able to alkylate Cys797 (i.e., afatinib, **2** and dacomitinib) allows to circumvent T790M-induced resistance [9], but at the cost of a marked toxicity due to the concurrent inhibition of $EGFR^{WT}$ [10]. Replacement of the 4-anilinoquinazoline nucleus of afatinib with a 2-anilinopyrimidine core [11] led to a third generation of TKIs, exemplified by rociletinib (CO-1686, **3**) [12] and osimertinib (AZD-9291, **4**) [13] that are able to potently and irreversibly block L858R/T790M and del19/T790M EGFR isoforms, while sparing $EGFR^{WT}$ and thus reducing side effects [14]. Osimertinib was approved for treatment of NSCLC patients harboring T790M mutation [15] and more recently has become the front-line treatment for NSCLC patients with activating mutations on EGFR [16].

T790M-positive NSCLC patients treated with osimertinib develop resistance through different mechanisms, which include both on-target and off-target alterations [17]. The most frequent acquired mutation occurring on-target is C797S mutation [18]. The replacement of Cys797 with a less reactive serine residue prevents the formation of covalent bond between EGFR and the acrylamide warhead, making osimertinib clinically ineffective [19]. In the current scenario, the discovery of inhibitors targeting EGFR C797S variants represents an urgent therapeutical need for the treatment of NSCLC.

Distinct medicinal chemistry strategies are currently being followed to identify fourth-generation EGFR inhibitors, which must be active on osimertinib-resistant C797S variants [20]. An effective approach is represented by reversible inhibitors undertaking tight interactions with the catalytic lysine (Lys745) and neighboring residues [21]. Illustrative classes of inhibitors exploiting this strategy are trisubstituted imidazoles [22], pyrimidopyrimidinones [23], pyridoindole [24] and macrocyclic aminobenzimidazoles [25], with the last two chemotypes including compounds able to induce tumor regressions in $EGFR^{del19/T790M/C797S}$ xenograft mice models. The detrimental effect of C797S mutation can also be overcome by allosteric inhibitors. These compounds recognize a back-pocket proximal to the ATP binding site, the size of which is controlled by the position of the αC-helix [26], stabilizing the inactive state of EGFR. However, the activity of this class of compounds is restricted to the $EGFR^{L858R/T790M/C797S}$ variant, while allosteric inhibitors fail to block the activity of $EGFR^{del19/T790M/C797S}$ mutant [27].

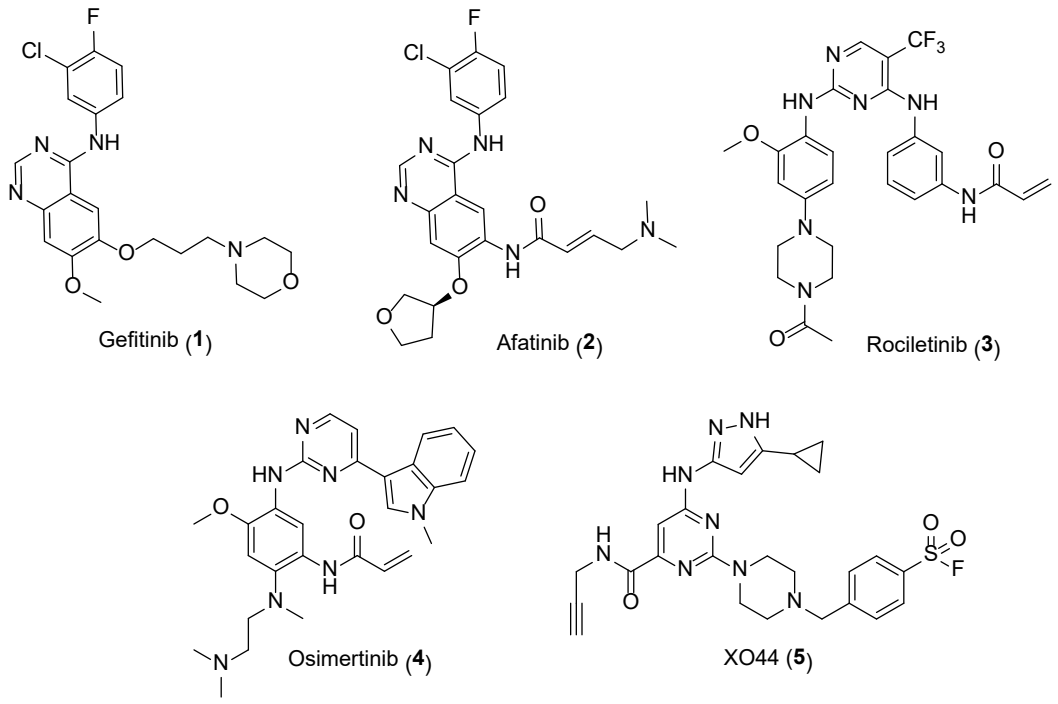

Fig. 1. Chemical structures of selected EGFR inhibitors.

An alternative option in the search for fourth-generation EGFR inhibitors is represented by covalent agents, particularly in light of the biochemical properties of T790M/C797S variants of EGFR which possess high affinity for ATP [28]. Covalent agents, being able to form a stable bond with the active site, can overcome competition with ATP and thus efficiently inhibit EGFR activity in cells and tissues [29]. This approach, however, requires the identification of a nucleophilic residue alternative to Cys797 featured by favorable properties [30]. This nucleophile should be *i.* proximal to the ATP binding site, *ii.* accessible to convenient warheads [31], *iii.* surrounded by an environment increasing reactivity [32], *iv.* featured by a fundamental biological role [33] so that it would be less prone to mutation than non-essential residues. The catalytic lysine of EGFR (and other kinases) complies with all these requirements and has thus emerged as “hot-spot” for covalent drug design.

In principle, different warheads could interact with the amine group of Lys745 [34] giving an alkyl or an acyl derivative, and the sulfonyl fluoride group has recently attracted interest as a potential sulfonylating agent of protein therapeutic targets [35]. Efforts in this direction have led to XO44 (**5**), a sulfonyl fluoride derivative able to covalently modify $EGFR^{L858R/T790M/V948R}$ by forming a sulfonamide bond with Lys745 [36]. When added to intact cells, XO44 modified 133 endogenous kinases [36], implying that the targeting of a highly conserved residue dramatically hampers selectivity. The marked promiscuity of XO44 could be attributed to: *i*. excessive reactivity of the sulfonyl fluoride warhead or *ii*. the presence of the 3-aminopyrazole scaffold that, being insensitive to the stereoelectronic properties of the "gatekeeper" residue within the ATP binding site [36], ensures the engagement of the vast majority of the kinome [37]. When a subtype-selective hinge binding scaffold is employed, promiscuity can be reduced [38] even with sulfur(VI) fluoride warheads [39].

The assessment of the potential of EGFR catalytic lysine as a targetable site to devise EGFR selective compounds overcoming C797S mutation and of the suitability of a sulfonyl fluoride warhead to this end requires the availability of a selective inhibitor active on osimertinib-resistant cell lines. Following the hypothesis that the lack of selectivity of XO44 is due to scaffold promiscuity, such a compound could result from the insertion of the sulfonyl fluoride on an EGFR-selective scaffold, adjusting the link geometry to favor the formation of a sulfonamide bond with Lys745.

We report here the design, synthesis and biochemical characterization of a class of 2-anilino-5-chloro-pyrimidine derivatives bearing warheads potentially able to form a covalent bond with Lys745. The ability of the compound to inhibit C797S variants of EGFR was assessed through a panel of enzymatic assays based on time-resolved fluorescence resonance energy transfer (TR-

FRET) technology, while the molecular mechanism of inhibition was elucidated through high-resolution mass spectrometry (HRMS). Finally, the most promising compound was evaluated for its ability to inhibit EGFR autophosphorylation and proliferation of Ba/F3 cells expressing $EGFR^{L858R/T790M/C797S}$ or $EGFR^{del19/T790M/C797S}$.

2. RESULTS AND DISCUSSION

2.1 Design and synthesis of 2-anilino-5-chloropyrimidines targeting $EGFR^{L858R/T790M/C797S}$

Potential EGFR inhibitors carrying electrophilic groups belonging to distinct chemical classes (Fig. 2) were designed linking the 2-anilinopyrimidine hinge binding scaffold, shared by third-generation EGFR-TKIs and known to confer selectivity versus EGFR T790M mutants [40], with a set of warheads (WAs) reported to react with free amines in solution or within a protein environment [31].

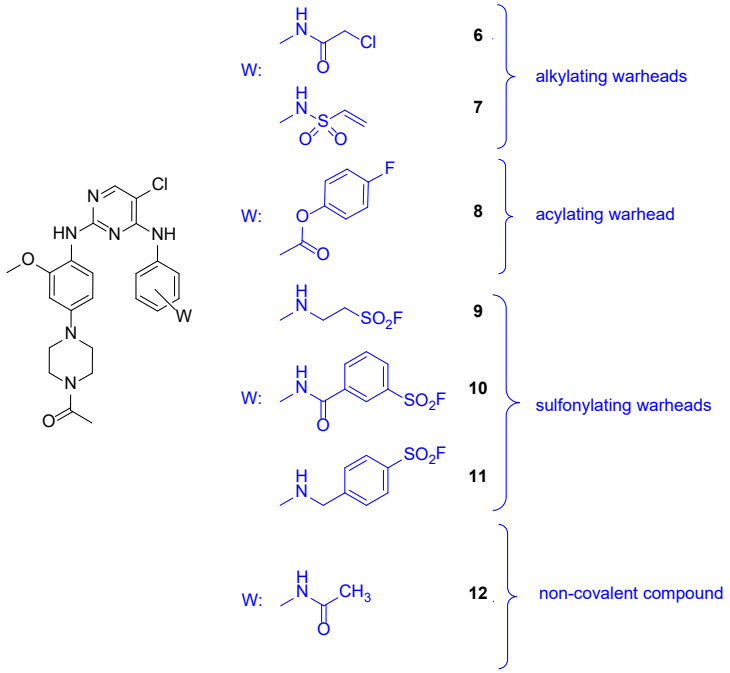

Fig. 2. Set of substituents installed on the 2-anilinopyrimidine hinge binding group of third-generation EGFR inhibitors.

The selected WAs might modify the catalytic lysine through different reaction mechanisms including *i.* alkylation [41] (chloroacetamide **6**, vinyl sulfonamide **7**), *ii.* acylation [42] (activated ester **8**) and *iii.* sulfonylation [43] (aliphatic or aromatic sulfonyl fluorides **9, 10** and **11**). A 2-anilinopyrimidine devoid of a reactive electrophilic centre (compound **12**) was prepared as prototypical non-covalent agent, to be used as a negative control in enzymatic assays.

The selection of the stereoelectronic properties of the linker connecting the WA to the peripheral aniline of the hinge binding scaffold was driven by docking simulations employing the X-ray coordinates of the kinase domain of $EGFR^{L858R/T790M/V948R}$ taken from the covalent adduct with XO44 (PDB code: 5U8L) [36]. In this X-ray structure, the activation loop and the αC-helix of the kinase domain assumes a catalytically inactive conformation creating a hydrophobic microenvironment around Lys745. Such a conformation may stabilize the neutral form of lysine basic group thus enhancing its nucleophilicity [44]. When docked into a model structure where the ligand had been deleted, XO44 placed its electrophilic centre at 4.0 Å from the nitrogen atom of Lys745 (Fig. 3A). Designed compounds placing the electrophilic centre at a distance not higher than 6 Å from Lys745 nitrogen while forming an H-bond with the hinge region of the kinase domain, similarly to rociletinib [45] and osimertinib [46] (see Table S1, Supplementary Data, SD, for details) were advanced to the synthesis. Representative models for synthetized compounds are reported in Fig. 3.

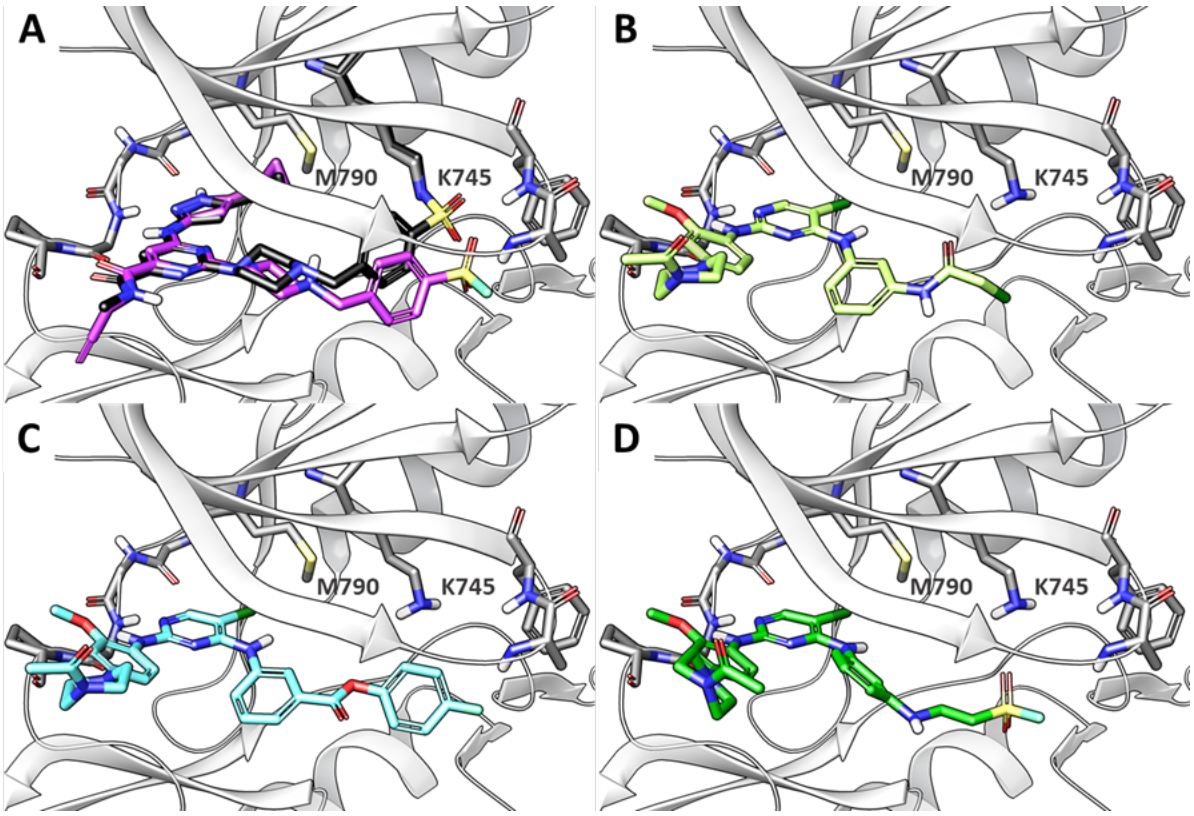

Fig. 3. Docking of selected compounds within $EGFR^{L858R/T790M/V948R}$ active site (white ribbons, grey carbon atoms). Important residues (M790, K745) or regions of EGFR (backbone of hinge region and p-loop turn) are displayed. Panel A reports the best-ranked docked pose for XO44 (pink carbon atoms) superposed on the experimentally observed EGFR-XO44 covalent adduct (black carbon atoms). Best docked poses for chloroacetamide **6** (panel B, lime carbon atoms), ester **8** (panel C, cyan carbon atoms) and aliphatic sulfonyl fluoride **9** (panel D, green carbon atoms).

The synthetic strategy adopted to obtain the EGFR inhibitors **6-12** is based on a convergent approach starting from commercially available 2,4,5-trichloropyrimidine (**13**) condensed regioselectively with either 3-nitro aniline to give the functionalized pyrimidine core **14a**, 4-nitro aniline to give **14b**, or 3-amino benzoic acid to give **14c** (Scheme 1). These were then subjected to a second condensation with the anilino-piperazine fragment **15** [47] and the nitro group was

finally reduced to furnish **17a**,**b**. Compound **16c** was condensed with 4-fluorophenol to give the activated ester **8**.

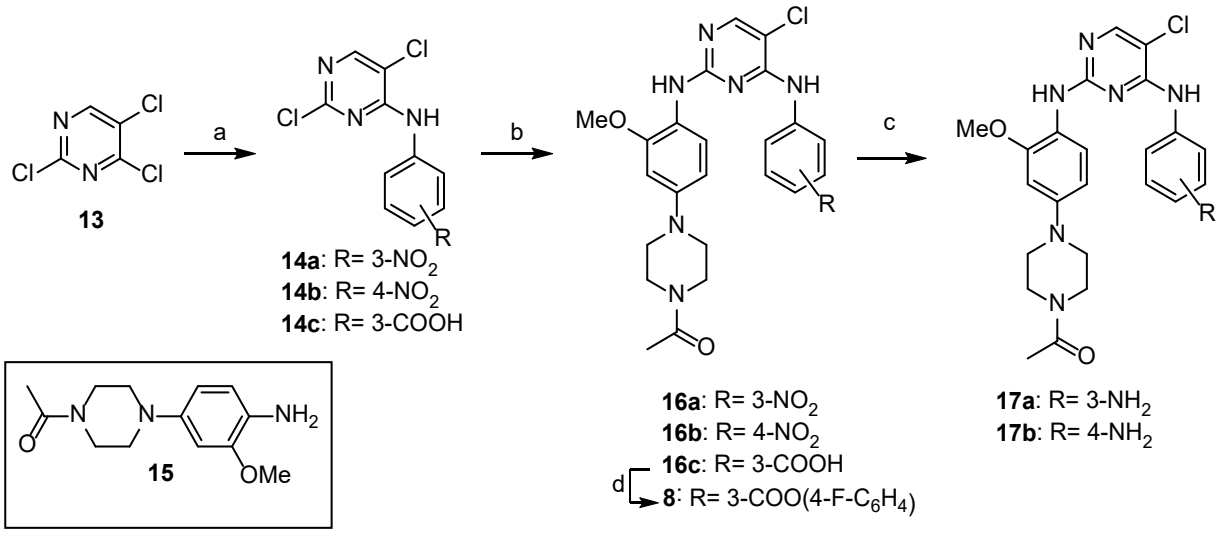

Scheme 1. a) HCl, water, reflux; b) **15**, iPrOH, p-TsOH, reflux; c) Zn^0, NH_4Cl, THF/water = 5:1, reflux,; d) 4-fluoro phenol, EDCI, triethylamine, THF, rt 88%.

The amino-functionalized scaffold **17a** was then elaborated to obtain the lysine-targeting inhibitors, by reacting with the electrophilic partner of choice (Scheme 2). Chloroacetamide-functionalized compound **6** was prepared employing the mixed anhydride between chloroacetic acid and trimethylacetic acid **18**. Vinylsulfonamide **7** was prepared by reacting **17a** with 2-bromoethane-1-sulfonyl chloride **19** (with concomitant elimination to yield the unsaturated compound) [48], while compound **9** resulted from the hetero-Michael addition of **17a** to commercially available ethenesulfonyl fluoride **20** [49] Compound **10** was obtained by acylation with 3-(fluorosulfonyl)benzoyl chloride **21**, prepared according to a literature procedure [50].

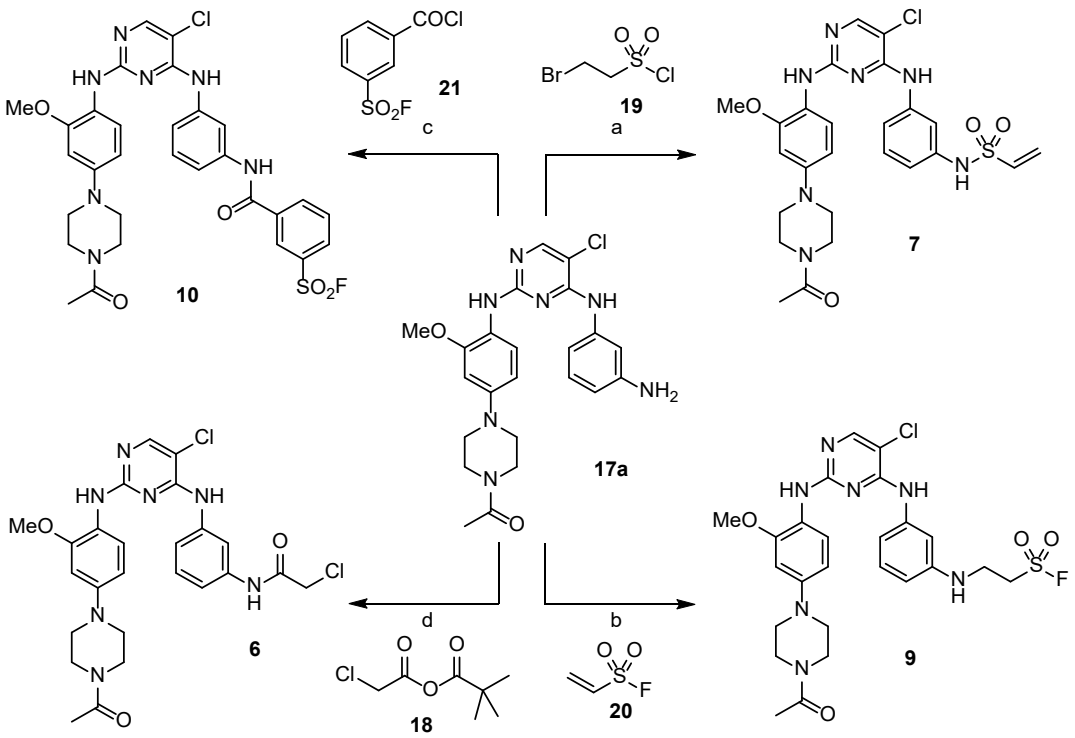

Scheme 2. a) triethylamine, THF, 0 °C to rt; b) chloroform, methanol, rt; c) pyridine, THF, 0 °C to rt; d) triethylamine, THF.

Compound **11** was obtained by alkylation of **17b** with 4-(bromomethyl)benzenesulfonyl fluoride, prepared with minor adaption to a reported procedure (Scheme 3) [51]. Finally, acetamide **12** was prepared by reacting **17a** with acetic anhydride in pyridine.

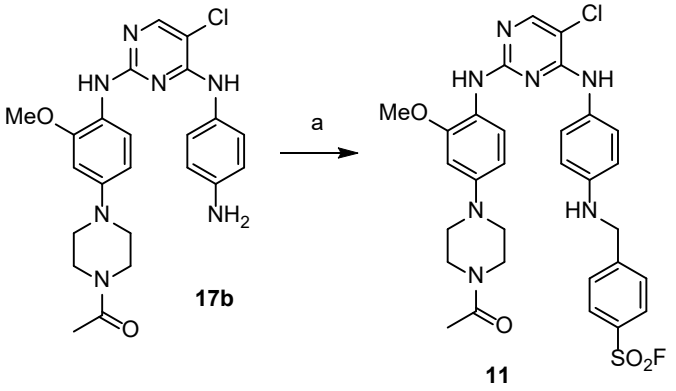

Scheme 3. a) 4-(bromomethyl)benzenesulfonyl fluoride, K_2CO_3, DMF, rt.

2.2 Inhibition of EGFR$^{L858R/T790M/C797S}$

A TR-FRET assay was setup to evaluate the ability of anilinopyrimidines **6-12** to inhibit the catalytic activity of recombinant EGFR bearing L858R/T790M/C797S triple mutation. Different concentrations of the title compounds (0.1 nM - 10 μM range) were co-incubated with enzyme, ATP (at a concentration equal to its Km value), and a fluoresceine-labelled poly-GT peptide for 1h. The reaction was thus quenched and the enzyme activity was measured monitoring TR-FRET signals generated by the association between the phosphorylated form of the labelled poly-GT peptide and an europium-labelled anti-phosphoTyr antibody added to the kinase buffer (see Experimental Section for details).

Half-maximal inhibitory concentrations (IC_{50}) for compounds **4-12** are reported in Table 1. Osimertinib weakly inhibited EGFR$^{L858R/T790M/C797S}$ displaying an IC_{50} of 430 nM, in line with literature data [22,23]. The sulfonyl derivative XO44 (**5**) resulted slightly more potent than osimertinib at inhibiting EGFR$^{L858R/T790M/C797S}$. Alkylating (**6** and **7**) and acylating (**8**) agents displayed low potency values, while sulfonyl fluorides **9-11** displayed IC_{50} values in line (**9**,**10**) or lower (**11**) than osimertinib.

Compound **12**, lacking a reactive warhead, displayed an IC_{50} value in the micromolar range. In this regard, the presence of a sulfonyl fluoride warhead in **9-11** appeared beneficial for EGFR$^{L858R/T790M/C797S}$ inhibition when installed on the 2-anilino-5-chloropyrimidine scaffold.

Table 1. Inhibitory potency (expressed as IC_{50}) on $EGFR^{L858R/T790M/C797S}$.

Compounds	Chemical structure	IC_{50} (nM)[a] on $EGFR^{L858R/T790M/C797S}$
4 (osimertinib)	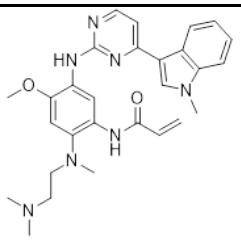	430 ± 24
5 (XO44)	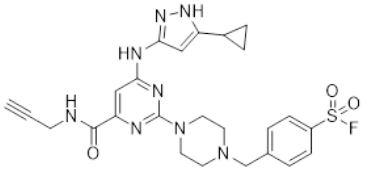	244 ± 77
6	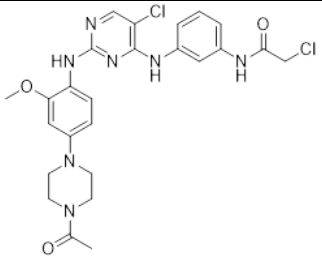	946 ± 28
7	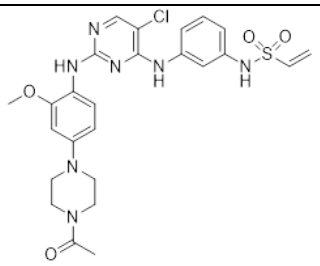	675 ± 150
8	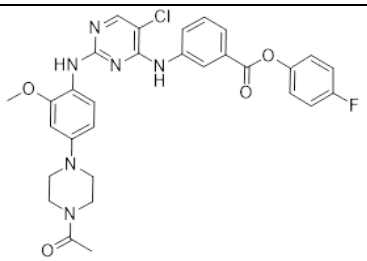	> 10,000[b]
9	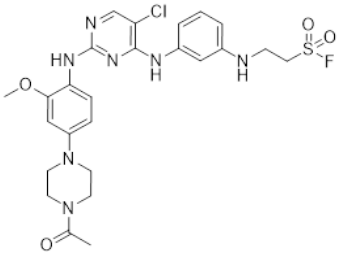	458 ± 12

10	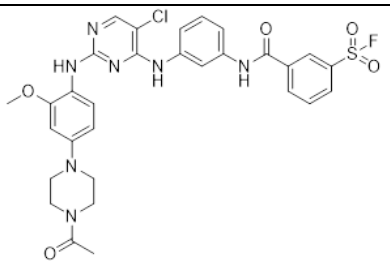	476 ± 51
11	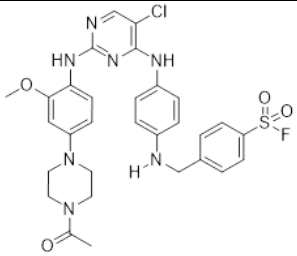	110 ± 33
12	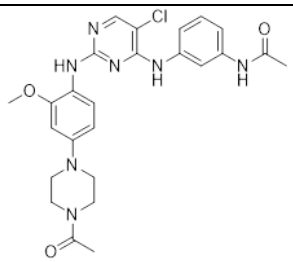	1,105 ± 48

[a] Measured by TR-FRET (see Experimental Section for details). IC_{50} values are reported as mean ± standard error of the mean (n = 5). [b] No inhibition observed up to 10,000 nM.

2.3 Time-dependency of inhibition on EGFR$^{L858R/T790M/C797S}$ and reversibility studies

Presuming a covalent interaction between EGFR$^{L858R/T790M/C797S}$, XO44 and sulfonyl fluorides **9**-**11**, we evaluated the time-dependency of their inhibitory potency. When a pre-incubation stage is introduced in an enzymatic assay, a reduction in the measured IC_{50} is observed, if a significant fraction of the enzyme is taken out from equilibrium by covalent labelling [52,53]. TR-FRET experiments were thus performed by pre-incubating XO44 or compounds **9**-**11** with EGFR$^{L858R/T790M/C797S}$ for 3h before adding ATP, the fluorescent poly-GT substrate, and then the europium-labelled anti-phosphoTyr antibody. The ALK-targeting drug brigatinib, recently reported to potently inhibit recombinant EGFR$^{L858R/T790M/C797S}$ [54], acetamide **12**, and osimertinib were included as controls.

Fig. 4 reports dose-response curves for the abovementioned sulfonyl fluorides. XO44 displayed a significant shift in the measured IC_{50} value (from 244 ± 77 nM to 6.0 ± 0.5 nM), with a 40-fold gain of inhibitory potency. Compounds **9** and **10** displayed negligible or moderate dependency of their potency on the time of pre-incubation, while sulfonyl fluoride **11** displayed a remarkable change in the inhibitory potency, with a measured IC_{50} value of 1.5 ± 0.2 nM, 70-times lower than that measured without pre-incubation. The inhibitory activity of compounds lacking warheads (brigatinib and **12**) was barely affected by pre-incubation. Brigatinib displayed IC_{50} values of 12.5 and 18.5 nM with or without enzyme pre-incubation, respectively. A similar behavior was displayed by acetamide **12** (Fig. S1 in the SD) which possessed IC_{50} values in the micromolar range in both conditions. Conversely, osimertinib does not inhibit $EGFR^{L858R/T790M/C797S}$ at any of tested concentration (up to10 μM) after 3h pre-incubation.

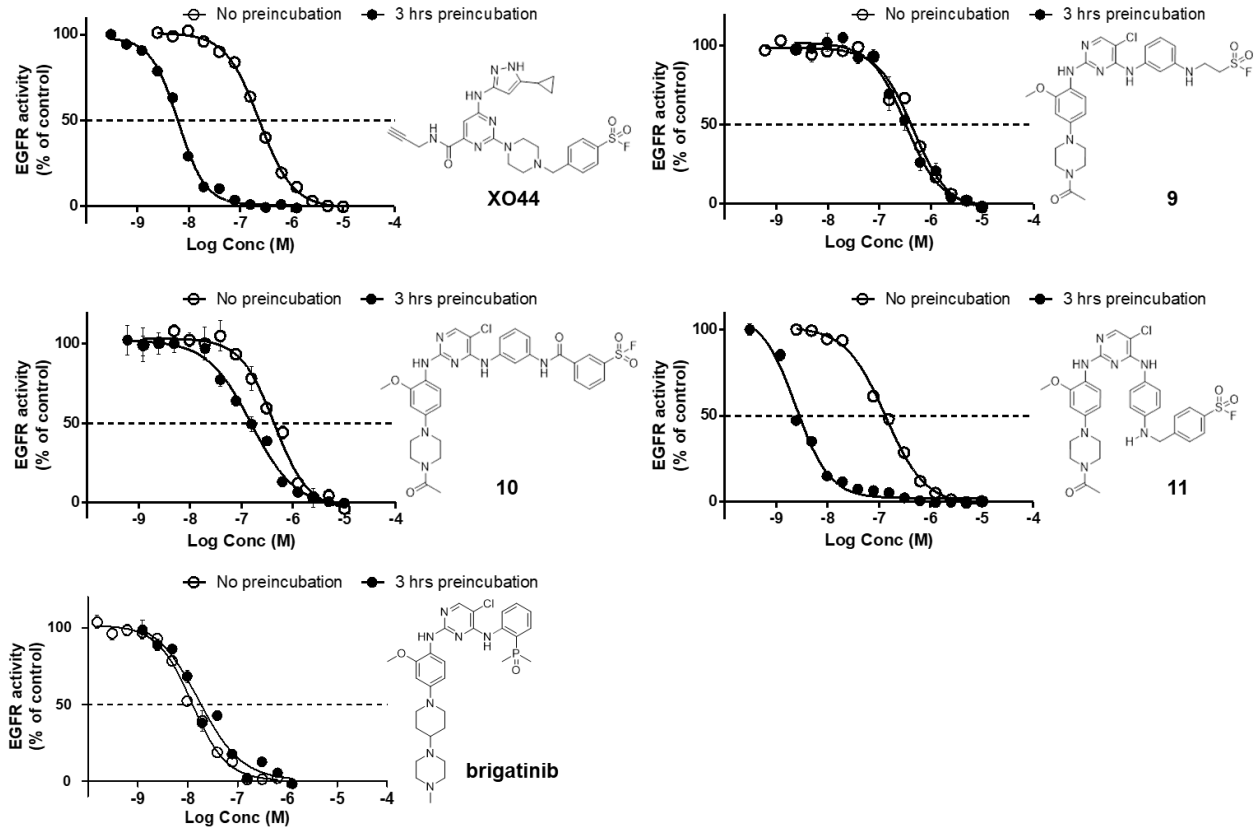

Fig. 4. Effect of the pre-incubation time on the dose-response inhibition curves for sulfonyl fluorides **5** (XO44), **9-11** on recombinant $EGFR^{L858R/T790M/C797S}$. Brigatinib is included as control. Kinase activity was measured by TR-FRET. Activity data are reported as mean ± standard error of the mean (n = 5).

TR-FRET experiments were also performed by pre-incubating sulfonyl fluoride **11** with $EGFR^{L858R/T790M/C797S}$ for 3h in the presence of ATP, either at its K_m (9 μM), or at a concentration 10-fold higher (90 μM). After this inhibitor/ATP co-incubation phase, a novel aliquot of ATP was added (at K_m concentration) together with the fluorescent poly-GT substrate. After 1h, the reaction was quenched and the enzyme activity was measured monitoring TR-FRET signals detected adding an europium-labelled anti-phosphoTyr antibody to the buffer.

Fig. 5 reports the dose-response inhibition curves for sulfonyl fluoride **11** obtained in these conditions along with the curve obtained pre-incubating **11** with $EGFR^{L858R/T790M/C797S}$ in absence of ATP. Gathered data indicate that compound **11** is able to potently inhibit $EGFR^{L858R/T790M/C797S}$ even when ATP is pre-incubated at a concentration equal to its K_m. In this conditions, the inhibitory potency of **11** reaches the low nanomolar range with an IC_{50} value (2.8 ± 0.7 nM), in line with the potency measured in absence of ATP (IC_{50} = 1.5 ± 0.2 nM). Conversely, when ATP is pre-incubated at concentration 10-fold the K_m value, a shift in the inhibitory dose response curve is observed, with a moderate drop in the inhibitory potency on $EGFR^{L858R/T790M/C797S}$ (IC_{50} = 23 ± 2 nM). Overall these data indicate that at high concentration ATP can effectively hamper the ability of sulfonyl fluoride **11** to engage $EGFR^{L858R/T790M/C797S}$ triple mutant.

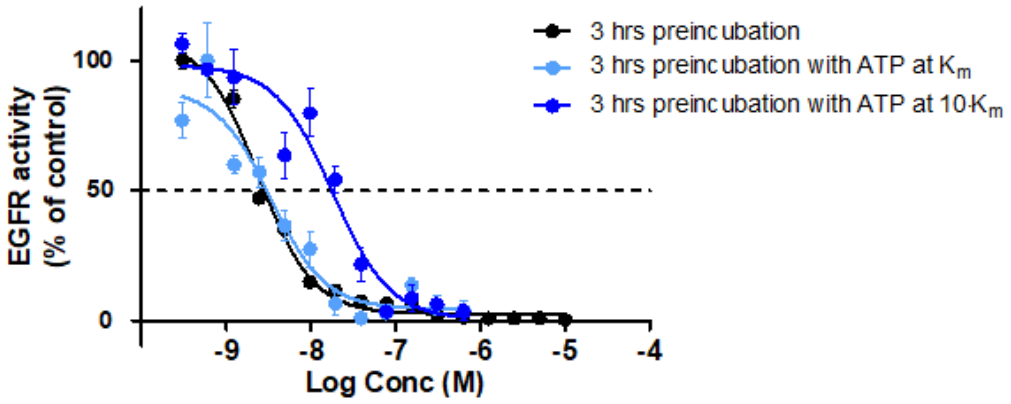

Fig. 5. Effect of ATP concentration of the dose-response inhibition curves for sulfonyl fluoride **11** on recombinant $EGFR^{L858R/T790M/C797S}$. No ATP (black curve), ATP at a concentration equal to the K_m value (cyan curve) or ATP at a concentration 10-fold the K_m value (blue curve) were pre-incubated with EGFR and **11** for 3h before adding poly-GT substrate**.** Kinase activity was measured by TR-FRET. Activity data are reported as mean ± standard error of the mean (n = 5).

The marked time dependency of the measured potency **11** indicates that this compounds might subtract $EGFR^{L858R/T790M/C797S}$ from equilibrium by sulfonylating its kinase domain. For compound **10**, the possibility to act as covalent modifier appears less likely. To evaluate the reversibility of triple mutant-EGFR inhibition, a rapid dilution assay was performed. $EGFR^{L858R/T790M/C797S}$ was pre-incubated for 3h with no inhibitor (control vehicle), with compound **10** or **11** in saturating conditions. Acetamide **12** and XO44 were added as negative and positive control, respectively. The samples were diluted in a kinase buffer (containing ATP and the poly-GT peptide) and the activity of the enzyme was measured by TR-FRET after addition of a europium-labelled anti-phosphoTyr antibody (see Experimental section for details).

The catalytic activity of $EGFR^{L858R/T790M/C797S}$ pre-incubated with acetamide **12** and sulfonyl fluoride **10** was fully recovered after dilution, (Fig. 6). When $EGFR^{L858R/T790M/C797S}$ was pre-incubated with XO44 or **11** only minor kinase activity was observed after dilution (< 25%) suggesting that both compounds act as irreversible inhibitors of $EGFR^{L858R/T790M/C797S}$.

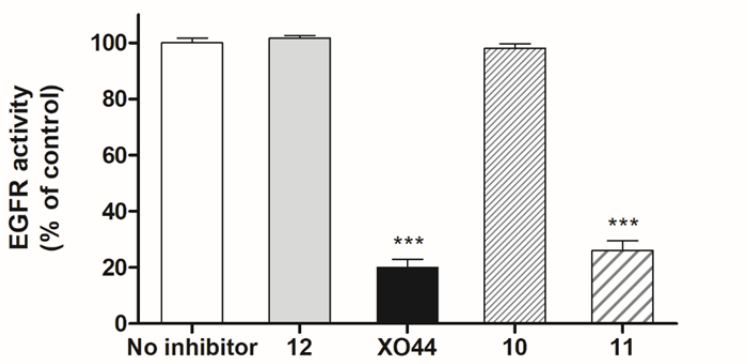

Fig. 6. Rapid dilution assay for $EGFR^{L858R/790M/C797S}$. The enzyme was pre-incubated for 3h with the titled compounds at ten times their IC_{50} values. The treated samples were diluted (100-fold) and the activity of the enzyme was assessed measuring the amount of phosphorylated poly-GT peptide 30 minutes after dilution by TR-FRET. Activity is reported as % of the control (no inhibitor). Data are reported as mean ± standard error of the mean (n = 5). Statistical significance vs No inhibitor was set at $p<0.05$. ***: $p<0.001$.

We speculated that compound **11** gives persistent inhibition of the kinase due to its ability to efficiently sulfonylate Lys745. Docking simulations suggest that this process might depend on the ability of **11** to form a non-covalent complex with $EGFR^{L858R/790M/C797S}$ similar to that given by XO44, with the electrophilic group well-positioned to react with Lys745 (Fig. 7A). Compound **10**, which can be docked into the ATP-binding site in a similar way (Fig. 7B), but allocating its sulfonyl fluoride group in a position not strictly superposed to that of XO44, does not irreversibly inhibit $EGFR^{L858R/T790M/C797S}$, probably due to a sub-optimal reaction geometry.

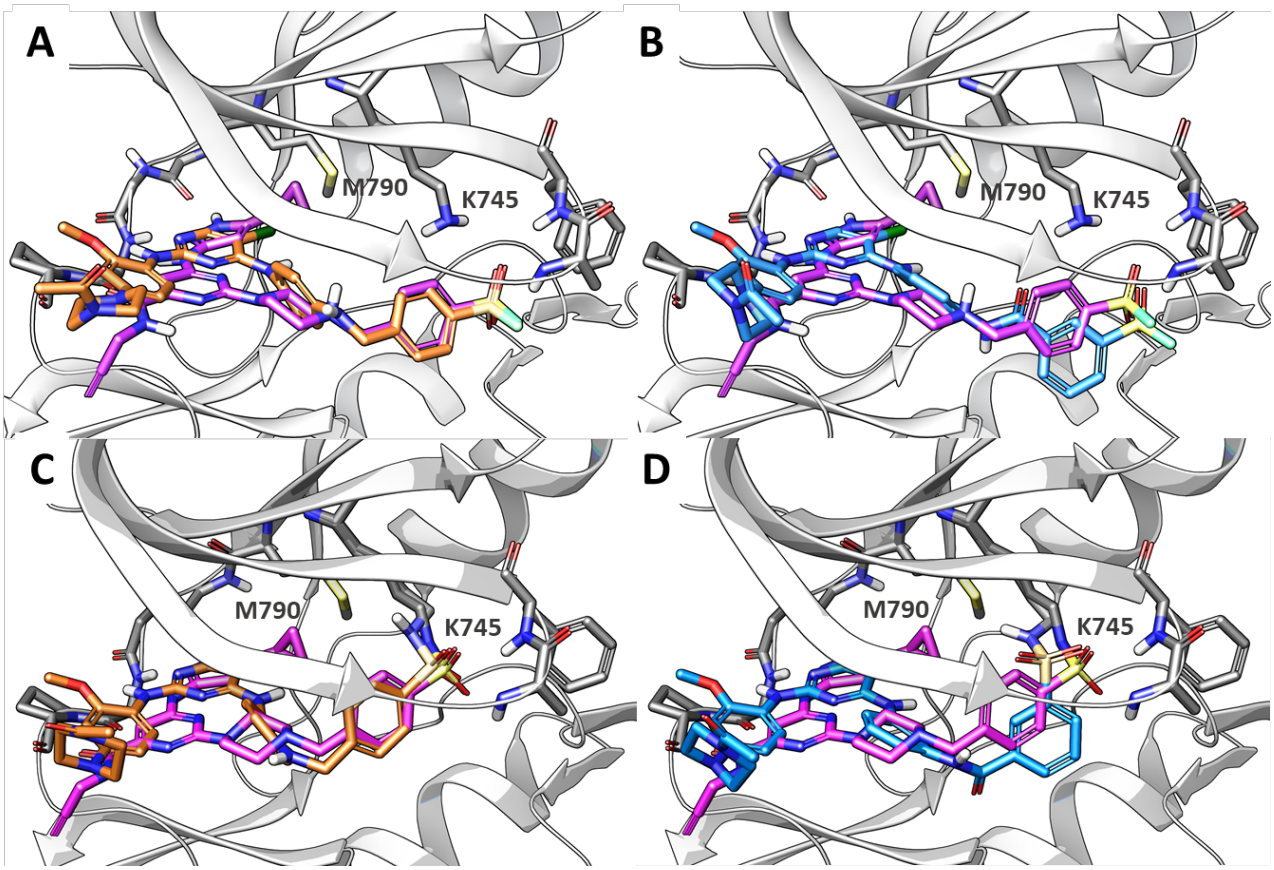

Fig. 7. Best docking (panels A, B) and best covalent docking (panels C, D) poses within EGFR L858R/T790M/V948R (white ribbons, grey carbon atoms) for aromatic sulfonyl fluorides **11** (panels A, C, orange carbon atoms) and **10** (panel B, D, blue carbon atoms). XO44 (pink carbon atoms) in its docked pose or in its covalent adduct with EGFR is reported for comparison.

To further characterize the different activity between sulfonyl fluorides **10** and **11,** covalent docking simulations were performed. The top-ranked poses are reported in Fig. 7C and 7D. While the hinge binding scaffold of **10** and **11** adopts the same binding mode, their phenylsulfonyl groups occupied slightly different regions of EGFR active site. Compound **11** well superposes its phenylsulfonyl portion on the same functional group of the co-crystallized inhibitor XO44 (Fig. 7C). In this covalent pose, **11** can form polar interactions with the p-loop, similarly to XO44. Compound **10** places its phenylsulfonyl group slightly far away from XO44

and from the NH groups of the p-loop. Also in energetic terms, sulfonyl fluoride **11** is predicted to bind EGFR with higher affinity (docking score = -9.9 kcal/mol) compared to **10** (docking score -9.1 kcal/mol), thus accounting for the different potency observed in the TR-FRET assay.

2.4 Mechanism of inhibition for compound 11 on EGFR$^{L858R/T790M/C797S}$ by LC-HRMS

To corroborate the hypothesis that compound **11** irreversibly inhibits EGFR$^{L858R/T790M/C797S}$ by forming a covalent bond with Lys745, a high-resolution mass spectrometry analysis of EGFR$^{L858R/T790M/C797S}$ in the presence of compound **11** was performed. Triple mutant EGFR, co-incubated with **11** (1:5 molar ratio) or with control vehicle (DMSO) for 1h was submitted to limited proteolysis by trypsin at 37°C. Analysis of the tryptic digest by LC-HRMS identified an ion trace corresponding to a peptide containing the catalytic lysine (IPVAIK^{745}ELR) covalently bound to compound **11** (Fig. 8A).

When EGFR$^{L858R/790M/C797S}$ was treated with control vehicle, the corresponding peptide was not found and trypsin digestion led to the formation of other two peptides containing Lys745 (IPVAIK^{745}, Fig. S2, Table S2 in the SD; VIKIPVAIK^{745}, Fig. S3, Table S3 in the SD) probably because lysine sulfonylation by **11** prevented the cleavage of the peptide bond between Lys745 and Glu746. This finding is consistent with the ability of trypsin to cleave peptide bonds involving basic amino acids.[55] MS/MS analysis of these two unmodified peptides confirmed their identity (Fig. S4, Tables S4-S5 in the SD). Throughout analysis of collected ion signals indicates that Lys745 is the only residue modified by compound **11**. However, as the tryptic digestion of EGFR$^{L858R/790M/C797S}$ covers only the 55% of the amino acidic sequence of the kinase domain (with 19 lysine residues identified out of 27), it is not possible to rule out if other lysine residues were sulfonylated by compound **11.** A list of the peptides containing unmodified

lysine residues of EGFR$^{L858R/790M/C797S}$ identified by our LC-HRMS analysis is reported in the Table S6 of the SD section.

Characterization of the modified IPVAIK^{745}ELR peptide by isotopic profiling confirmed that it was covalently bound to compound **11**, with a theoretical mass for the $[M+3H]^{3+}$ ion identical to the experimental one (Fig. 8B) and an estimated error of only -0.4 mDa (-0.78 ppm). MS/MS analysis of the peptide sequence showed that sulfonylation specifically occurred at the basic nitrogen of Lys745 (Fig. S5, Table S7, in the SD). Compound **11** thus emerged as irreversible inhibitor of EGFR$^{L858R/T790M/C797S}$ able to selectively sulfonylate its catalytic lysine.

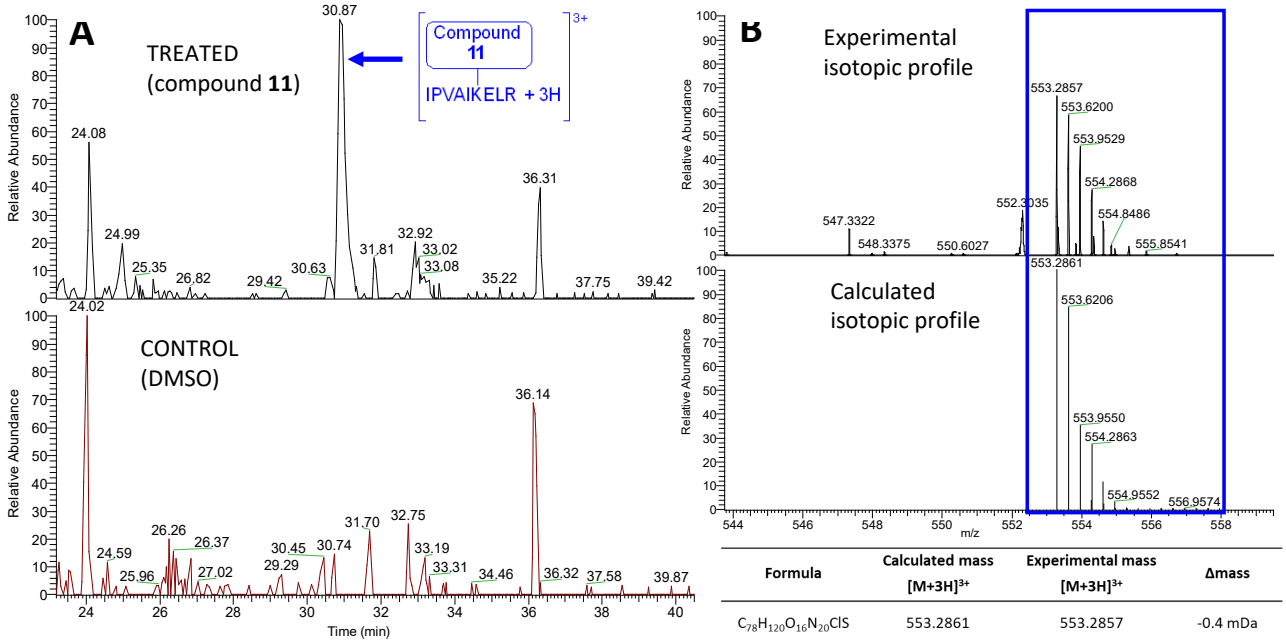

Fig. 8. LC-HRMS analysis for EGFR$^{L858R/T790M/C797S}$ treated with compound **11.** A) Extracted Ion Chromatograms in ESI^{+} of the triply charged $[M+3H]^{3+}$ ion corresponding to the Lys745-containing peptide modified by **11**. B) Mass and isotopic distribution in ESI^{+} for the $[M+3H]^{3+}$ ion of the modified Lys745-containing peptide.

2.5 Inhibition activity on EGFR$^{del19/T790M/C797S}$ and EGFR^{WT} of compound 11

In light of the activity of compound **11** on $EGFR^{L858R/T790M/C797S}$, we set to investigate its ability to interfere with activity of two other clinically relevant isoforms, the del19/T790M/C797S variant and the wild-type. When we tested the ability of **11** to inhibit $EGFR^{del19/T790M/C797S}$ with a TR-FRET kinase assay, it resulted inactive at all the tested concentrations (1 nM - 10 μM range) even with 3h inhibitor pre-incubation (Fig. S6). In the same conditions, also XO44 failed to inhibit $EGFR^{del19/T790M/C797S}$ kinase activity up to 10 μM. Conversely, osimertinib dose-dependently inhibited $EGFR^{del19/T790M/C797S}$ giving an IC_{50} value of 330 nM (Fig. S7, in the SD), in line with the results obtained on $EGFR^{L858R/T790M/C797S}$.

We speculate that **11** and XO44 do not inhibit $EGFR^{del19/T790M/C797S}$ because these compounds target an inactive state of the kinase which might not be accessible in the del19/T790M/C797S variant. Deletion of the E746-A750 peptide in $EGFR^{del19/T790M/C797S}$ is supposed to stabilize an active conformation of the kinase, [2] in which the αC-helix assumes an inward disposition with Lys745 engaged in two salt bridges, one with Asp855 of the DFG motif, the other with Glu762 of the same αC-helix, and thus not prone to react with electrophilic warheads. The inability of $EGFR^{del19/T790M/C797S}$ to assume an inactive state has been also proposed to justify the lack of activity of allosteric compounds on this specific mutant [27].

We then evaluated the ability of compound **11** to interfere with kinase activity of $EGFR^{WT}$, using the same TR-FRET assay employed for $EGFR^{L858R/T790M/C797S}$ and $EGFR^{del19/T790M/C797S}$. In this set of experiments, gefitinib (**1**) and osimertinib (**4**) were included as control compounds. IC_{50} values obtained are summarized in Table 2. Gefitinib (**1**) resulted highly potent on $EGFR^{WT}$ with an IC_{50} value reaching the sub-nanomolar range, in line with literature data.[40] Osimertinib and compound **11** were significantly less potent than **1** by 10- and 650- fold, respectively, which

is in line with the wild-type sparing character of covalent anilinopyrimidine-based EGFR inhibitors.

Table 2. Inhibitory potency (IC_{50}) on recombinant $EGFR^{WT}$.

Compounds	IC_{50} (nM)[a] (no pre-incubation)	IC_{50} (nM)[a] (3h pre-incubation)	IC_{50} Ratio
1 (gefitinib)	0.32 ± 0.1	0.1 ± 0.01	3.2
4 (osimertinib)	3.4 ± 1.0	0.62 ± 0.16	5.5
11	210 ± 50	30 ± 4.8	7.0

[a]Measured by TR-FRET. IC_{50} values are reported as mean ± standard error of the mean (n = 3).

Activity assays were also performed pre-incubating for 3h the titled inhibitors with $EGFR^{WT}$ before adding ATP to the kinase buffer. As expected, inhibitor pre-incubation marginally affected the inhibitory potency of gefitinib. The IC_{50} values of osimertinib and sulfonyl fluoride **11** displayed higher dependence on pre-incubation, even if that of **11** was lower than what observed on the L858R triple mutant (Fig. 4).

In a rapid dilution assay, $EGFR^{WT}$ was pre-incubated for 3h with no inhibitor (control vehicle), gefitinib (**1**), osimertinib or **11**. The samples were then diluted in a kinase buffer and the activity of the enzyme was measured by TR-FRET. The catalytic activity of $EGFR^{WT}$ pre-incubated with gefitinib (**1**) was fully recovered after dilution (Fig. 9). When $EGFR^{WT}$ was treated with osimertinib or **11**, the kinase activity was only partially recovered after dilution (40% and 60%, respectively), suggesting that both compounds likely modify only a fraction of the available binding sites in $EGFR^{WT}$.

The sulfonyl fluoride warhead on the 2-anilinopyrimidine scaffold has an impact on $EGFR^{WT}$ inhibition which parallels that of the acrylamide group of osimertinib. Either way, even after pre-

incubation the IC_{50} values of osimertinib and sulfonyl fluoride **11** are significantly higher than that of gefinitib, by 6- and 300-fold, respectively.

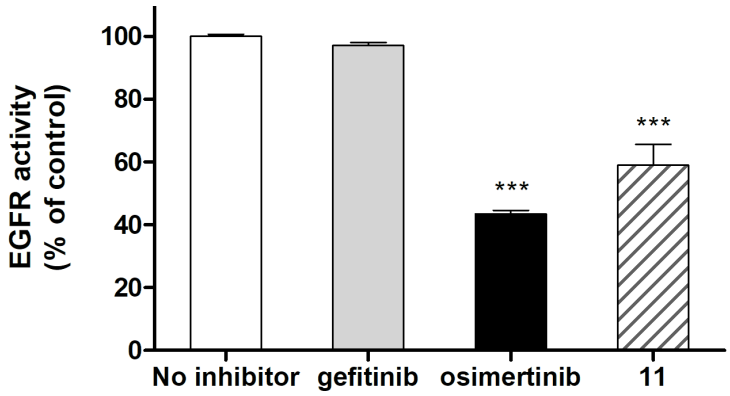

Fig. 9. Rapid dilution assay for gefitinib, osimertinib and **11**. $EGFR^{WT}$ was pre-incubated for 3h with the titled compounds ten times their IC_{50} values. The treated samples were diluted (x100) and the activity of the enzyme was assessed measuring the amount of phosphorylated poly-GT peptide 30 minutes after dilution by TR-FRET. Activity is reported as % of the control (No inhibitor). Statistical significance *vs.* No inhibitor was set at $p<0.05$. ***: $p<0.001$.

2.6 Selectivity versus other kinases

To further characterize the biochemical profile of compound **11**, we evaluated its selectivity potential by testing it on a panel of sixteen kinases which included serine-threonine (AKT2, AMP-K, aurora kinase A, CDK2, CDK5) and tyrosine kinases (BLK, LCK, SRC) reported to be significantly inhibited by XO44 [36] (Fig. 10A) and serine-threonine (ERK1, IKKβ, p38α, ROCK1) and tyrosine kinases (FGFR4, JAK1, PDGFRα, VEGR2) reported to be spared by XO44 [36] (Fig. 10B). A TR-FRET assay based on the Z'-LYTE™ technology was employed in this case. XO44 and acetamide **12** were included as controls.

As expected, XO44 had a dramatic impact on the activity of the first set of kinases (Fig. 10A), reaching very high (90%; AKT-2, CDK5) or full inhibition (AMP-K, aurora kinase A, CDK2, BLK, LCK, SRC) when tested at 1 μM. Also at 100 nM concentration, XO44 significantly inhibited these eight kinases, with five of them showing 90% inhibition or more. On the same set of enzymes, compound **11** was significantly less active than XO44 at both tested concentrations (Fig. 10A). At 100 nM, only aurora kinase A (AURKA) was moderately inhibited (30%), while all the other kinases were barely affected by this compound. On this group of XO44-sensitive kinases, acetamide **12** (tested at 1 μM) displayed a negligible inhibitory activity, similar to that observed for sulfonyl fluoride **11**.

On the second set of kinases (Fig. 10B), XO44 did not displayed inhibitory activity, in line with literature data [36]. Sulfonyl fluoride **11** displayed significant inhibitory activity only on JAK1, while it spared all the other kinases included in this set of enzymes (inhibitory activity < 25% at 1 μM). Acetamide **12** displayed some inhibitory activity only on JAK1, PDGFRα, and VEGR2 while it resulted inactive on all the other kinases.

Overall, these experiments suggest that the hinge binding scaffold has a major role in controlling selectivity and that the installation of a sulfonyl fluoride warhead does not necessarily confer promiscuity for the kinome.

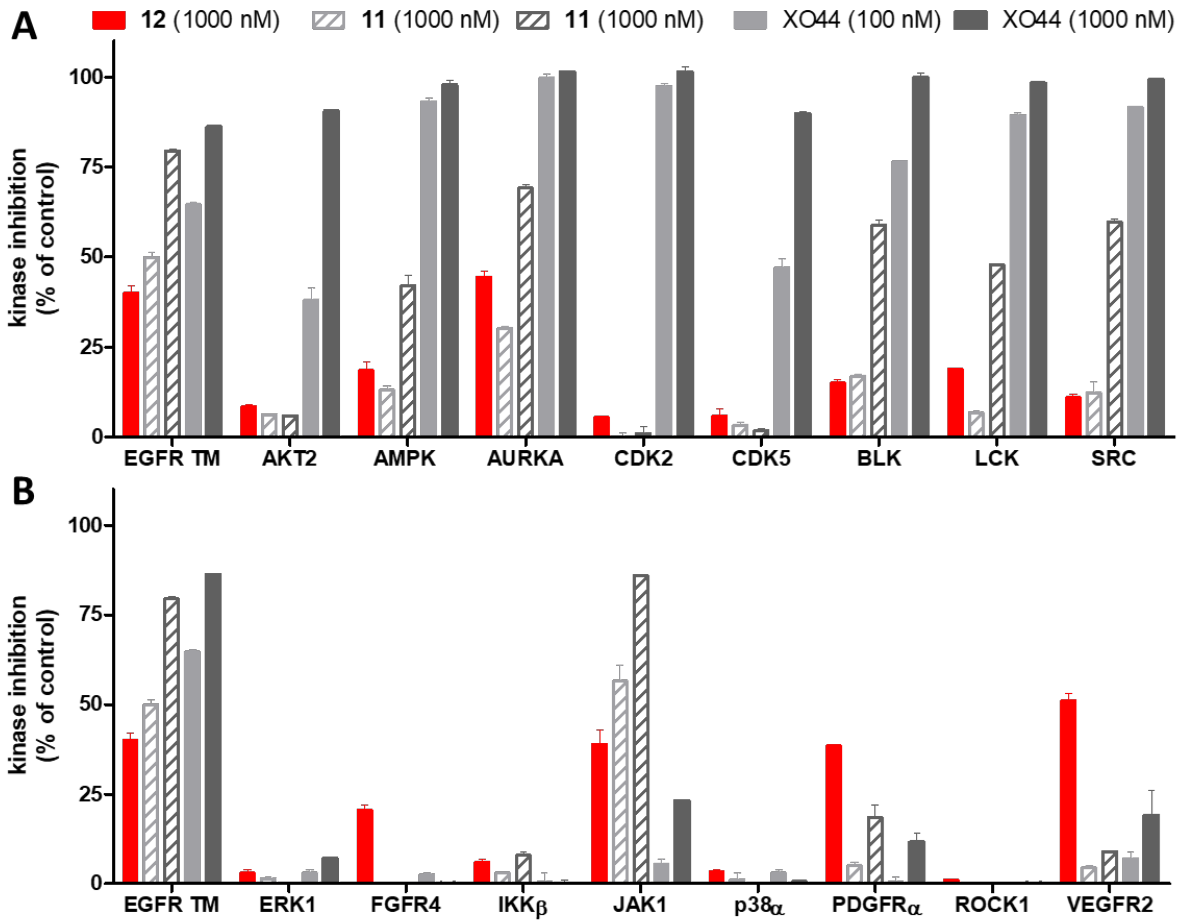

Fig. 10. Selectivity panel for compound **11** on kinases sensitive (panel A) or not sensitive (panel B) to XO44. Acetamide **12** was used as control. Compound **11** and XO44 were tested at 0.1 or 1 μM while acetamide **12** was tested at 1 μM. A Z'-LYTE^{TM} kinase assay was applied. EGFR TM stands for EGFR$^{L858R/T790M/C797S}$. Reported data represent the means of two independent experiments together with their standard deviations.

2.7 Biological activity of compound 11 in Ba/F3 cells expressing C797S EGFR variants

As final step of our investigation we evaluated the ability of compound **11** to interfere with EGFR activation in Ba/F3 cells expressing $EGFR^{L858R/T790M/C797S}$ or $EGFR^{del19/T790M/C797S}$. Osimertinib and XO44 were included in the analysis. Fig. 11A and 11B shows that 1 μM osimertinib did not interfere with EGFR phosphorylation (stimulated by EGF) in both the cell models. Compound **11** and XO44 significantly inhibited $EGFR^{L858R/T790M/C797S}$ phosphorylation at 1 μM (Fig. 11A) while they did not affect $EGFR^{del19/T790M/C797S}$ activity (Fig. 11B), in line with TR-FRET data on recombinant enzymes. The ability of compound **11** to inhibit $EGFR^{L858R/T790M/C797S}$ phosphorylation was dose-dependent and it was almost complete at the concentration of 500 nM (Fig. 11C).

The persistence of $EGFR^{L858R/T790M/C797S}$ inhibition was evaluated by measuring receptor autophosphorylation after removal of the inhibitor from the cellular medium. Ba/F3 cells were exposed to 1 μM of compound **11** for 4 h, washed with a buffer solution, and then incubated in a drug-free medium for 2, 4 or 8h before stimulation with EGF (Fig. 11D). Full recovery of $EGFR^{L858R/T790M/C797S}$ autophosphorylation was observed at all time points suggesting that in this cell line, the inhibitory activity displayed by **11** should be ascribed to a reversible mechanism. We speculate that ATP, which in cells is present at millimolar concentration, competes with compound **11** for the same binding site hampering the formation of a covalent bond between Lys745 and the sulfonyl fluoride warhead. Pre-incubation experiments on recombinant $EGFR^{L858R/T790M/C797S}$ with a TR-FRET assay are supportive of this notion, as high concentrations of ATP dramatically affected the ability of **11** to bind the kinase domain of this triple mutant (Fig. 5).

We finally examined the effect of compound **11** on cell viability by MTS assay, with XO44 and osimertinib used as control (Fig. 11C). Compound **11** was significantly more potent than

osimertinib at inhibiting cell proliferation in Ba/F3 cells expressing $EGFR^{L858R/T790M/C797S}$ (IC_{50} of 500 nM and more than 3,000 nM), respectively, in line with the inhibitory activity displayed on $EGFR^{L858R/T790M/C797S}$ autophosphorylation on the same cell line. Neither **11** nor osimertinib significantly affected viability of Ba/F3 cells expressing $EGFR^{del19/T790M/C797S}$ consistent with their substantial inactivity on $EGFR^{del19/T790M/C797S}$ triple mutant. The poor activity of **11** on Ba/F3 cells expressing $EGFR^{del19/T790M/C797S}$ suggests that no other targets relevant for cell growth are inhibited by this compound.

The pan-kinase derivative XO44 potently inhibited proliferation in Ba/F3 cells expressing $EGFR^{L858R/T790M/C797S}$ or $EGFR^{del19/T790M/C797S}$ regardless to its effect on EGFR autophosphorylation, which suggests that other kinases crucial for proliferations are inhibited by this poorly selective compound in this cell line. Also in Ba/F3 cell lines, sulfonyl fluoride **11** results more selective that XO44.

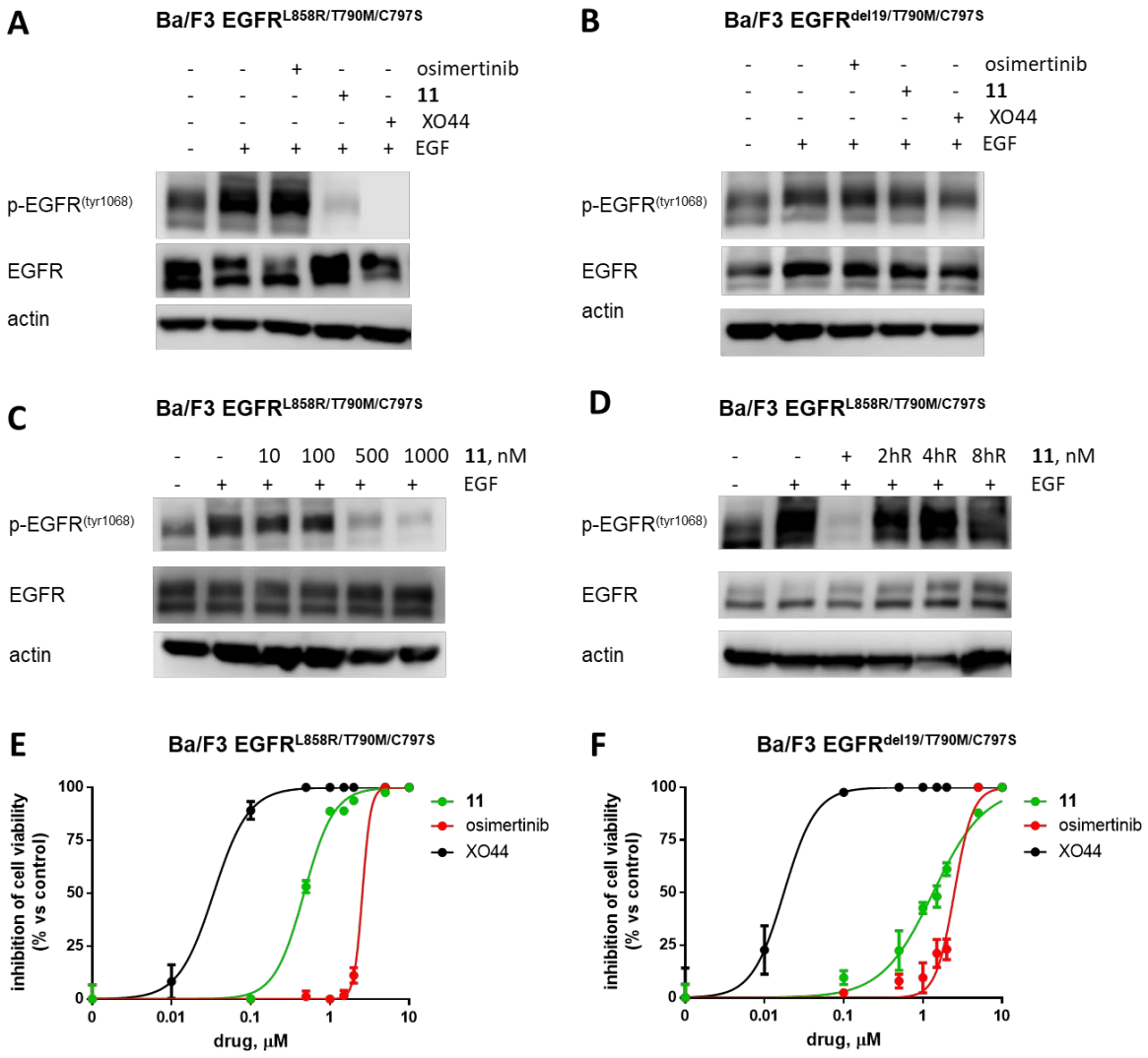

Fig. 11. Effects of compound **11** on EGFR phosphorylation and cell viability. Ba/F3 cells expressing EGFR$^{L858R/T790M/C797S}$ (panel A) or EGFR$^{del19/T790M/C797S}$ (panel B) were treated with **11**, osimertinib or XO44 at 1 µM for 4h and then stimulated with 100 ng/ml EGF for 10 min. EGFR phosphorylation was measured on lysate proteins by western blotting. Representative blots of two independent experiments are shown. C) Ba/F3 cells expressing EGFR$^{L858R/T790M/C797S}$ were treated with increasing concentration of compound **11** for 4h and then stimulated with 100 ng/ml EGF for 10 min. The expression of the indicated proteins was analyzed by western blotting. D) Ba/F3 cells expressing EGFR$^{L858R/T790M/C797S}$ were treated with

1 μM **11** for 4h and then stimulated with 100 ng/ml EGF for 10 min, or after 4h drug exposure, extensively washed with PBS and stimulated with EGF for 10min after 2, 4, or 8h of recovery (R) in fresh drug-free medium. Ba/F3 cells expressing $EGFR^{L858R/T790M/C797S}$ (panel E) or $EGFR^{del19/T790M/C797S}$ (panel F) were treated with increasing concentration of **11**, osimertinib and XO44. After 72h cell viability was evaluated by MTS assay and was expressed as % of inhibition versus untreated control cells. Results are representative of three independent experiments.

3. CONCLUSIONS

While osimertinib is an effective therapeutic option for NSCLC patients harboring activating mutation on EGFR, with or without T790M gatekeeper alteration, the insurgence of C797S variant abolishes its efficacy [1,2]. Different classes of compounds have been recently reported to inhibit C797S EGFR variants operating through non-covalent mechanisms. Analysis of their binding modes reveals that many of these compounds take polar interactions with Lys745, suggesting that targeting the catalytic lysine might be beneficial for improving potency on C797S EGFR variants [21]. Crucially, Lys745 can be efficiently targeted by TKIs bearing sulfonyl fluoride groups, as in the case of the pan-kinase inhibitor XO44 that sulfonylates the catalytic lysine of $EGFR^{L858R/T790M/V948R}$, as observed by X-ray crystallography [36].

In the present work, we have shown that covalent modification of Lys745 by a sulfonyl fluoride is a viable strategy to overcome the detrimental effect of C797S mutation in the case of $EGFR^{L858R/T790M/C797S}$ variant. Inspired by the activity of XO44, for the first time reported here to inhibit $EGFR^{L858R/T790M/C797S}$, we designed and synthetized a set of electrophilic compounds

potentially able to form a covalent bond with Lys745, featuring a 2-anilinopyridimine hinge-binding scaffold.

Among the synthesized compounds, the sulfonylating agent **11** (UPR1444) emerged as the most promising compound, able to irreversibly inhibit $EGFR^{L858R/T790M/C797S}$ by covalent modification of the catalytic Lys745. Remarkably, the sulfonylating agent **11** (and XO44) failed to inhibit triple mutant $EGFR^{del19/T790M/C797S}$. Furthermore, when tested on a panel of kinases (with many fully inhibited by XO44), compound **11** showed negligible or low inhibition, confirming that, also in the case of sulfonyl fluoride derivatives, selectivity can be modulated with the selection of a suitable hinge binding scaffold [38].

Our work shows that combination of a suitable scaffold and a reactive warhead targeting Lys745 can provide inhibition of $EGFR^{L858R/T790M/C797S}$ in cell-free environments and antiproliferative activity on osimertinib-resistant cell lines. On the other hand, the promising potential of sulfonyl fluorides still requires more investigations to be fully assessed. Several issues could limit the role of this warhead for drug development, such as chemical and metabolic stability or target selectivity. Moreover, as shown by the short-lasting effect in Ba/F3 cells, competition with ATP could hamper irreversible inhibition. Further optimization of the recognition portion and of the reactive warhead should be addressed toward a combination which may result more effective in Lys745 sulfonylation, which in turn strongly depends on the geometry of the interactions taken at the binding site, as shown by the present results on a 2-anilino-pyrimidine scaffold.

4. EXPERIMENTAL SECTION

4.1 Chemistry

All chemicals were obtained from commercial suppliers and used without further purification. Solvents were purified and stored according to standard procedures. Anhydrous reactions were conducted under a positive pressure of anhydrous N_2. Reactions were monitored by TLC, on Merck silica gel 60 F254 plates. Final compounds and intermediates were purified by column chromatography under "flash" conditions using Merck 230−400 mesh silica gel. Melting points were determined on a Gallenkamp melting point apparatus and are uncorrected. ^{1}H NMR and ^{13}C NMR spectra were recorded on a Bruker AVANCE, 300 or 400 instrument. Chemical shifts (δ scale) are reported in parts per million (ppm) relative to the central peak of the solvent. ESI-MS spectra of the final products were acquired on a Thermo TSQ Quantum Access Max triple quadrupole mass spectrometer (Thermo, San Jose, CA, USA) equipped with a heated electrospray ionization (H-ESI) source. The purity of tested compounds, determined by high performance liquid chromatography and mass spectrometry (HPLC-MS), was greater than 95%. The sulfonyl fluoride probe XO44 (compound **5**) was purchased by Sigma-Aldrich (Sigma-Aldrich, Milan, Italy), while brigatinib was purchased Selleckchem (Selleckchem, Houston, TX, USA).

*4.1.1 2,5-Dichloro-N-(3-nitrophenyl)pyrimidin-4-amine (**14a**).* 2,4,5-trichloropyrimidine (2.89 g, 15.76 mmol) and 3-nitroaniline (1.45 g, 10.51 mmol) are suspended in *i*-PrOH (30 ml). HCl (12 M, 1.3 ml, 15.6 mmol) is added and the mixture is stirred at 80 °C for 3 h. The yellow precipitate obtained (product **14a,** 2.17 g, 72%) is filtered and dried. ^{1}H NMR (400 MHz, $CDCl_3/CD_3OD$) δ 8.59 (t, J = 2.2 Hz, 1H), 8.21 (s,

1H), 8.04 (ddd, *J* = 8.2, 2.2, 1.0 Hz, 1H), 7.99 (ddd, *J* = 8.2, 2.3, 1.0 Hz, 1H), 7.55 (t, *J* = 8.2 Hz, 1H).

*4.1.2 2-((2-Methoxy-4-(4-acetylpiperazin-1-yl)phenyl)amino)-4-(((3-nitro)phenyl)amino)-5-chloropyrimidine (**16a**).* Compound **14a** (2.17 g, 7.61 mmol) and aniline **15** (1.26 g, 5.05 mmol) are suspended in *i*-PrOH (50 ml). PTSA*H_2O (1.92 mmol, 10.09 mmol) is added and the mixture is stirred at 80 °C for 15 h. The suspension is then cooled to room temperature and diluted with AcOEt, washed with $NaHCO_3$ and brine. After drying in the air, the title compound (1.26 g, 50%) is obtained as a brown solid. ^{1}H NMR (300 MHz, $CDCl_3$/CD_3OD) δ 8.54 (t, *J* = 2.2 Hz, 1H), 8.01 (s, 1H), 7.93 (dd, *J* = 7.8, 2.1 Hz, 1H), 7.87 (dt, *J* = 7.9, 1.5 Hz, 1H), 7.81 (d, *J* = 8.7 Hz, 1H), 7.47 (t, *J* = 8.2 Hz, 1H), 6.52 (d, *J* = 2.5 Hz, 1H), 6.33 (dd, *J* = 8.7, 2.5Hz, 1H), 3.84 (s, 3H), 3.73 (t, *J* = 5.2 Hz, 2H), 3.63 (t, *J* = 5.1 Hz, 2H), 3.09 (dt, *J* = 13.9, 5.2 Hz, 4H), 2.12 (s, 3H).

*4.1.3 2-((2-Methoxy-4-(4-acetylpiperazin-1-yl)phenyl)amino)-4-(((3-amino)phenyl)amino)-5-chloropyrimidine (**17a**).* Compound **16a** (1.10 g, 2.21 mmol) is dissolved in THF (150 ml). Zinc powder (1.24 g, 22.17 mmol) and NH_4Cl 1M in water (5 ml, 5 mmol) are added and the mixture is heated at reflux for 2 h. It is then cooled to room temperature and filtered on a pad of celite. The solvent is removed under reduced pressure and the residue is purified in a short silica column (AcOEt : MeOH = 9:1) to afford the title compound (965 mg, 93%) as a white solid. ^{1}H NMR (400 MHz, $CDCl_3$/CD_3OD) δ 8.00 (d, *J* = 8.8 Hz, 1H), 7.91 (s, 1H), 7.10 – 7.03 (m, 2H), 6.86 (ddd, *J* = 8.1, 2.1, 0.9 Hz, 1H), 6.56 (d, *J* = 2.6 Hz, 1H), 6.54 – 6.43 (m,

2H), 3.85 (s, 3H), 3.78 – 3.69 (m, 2H), 3.65 (t, *J* = 5.2 Hz, 2H), 3.10 (dt, *J* = 14.4, 5.1 Hz, 4H), 2.13 (s, 3H).

*4.1.4 2,5-dichloro-N-(4-nitrophenyl)pyrimidin-4-amine (**14b**).* 2,4,5-trichloropyrimidine (400 mg, 2.2 mmol) and 4-nitroaniline (1.45 g, 10.51 mmol) are suspended in *i*-PrOH (30 ml). HCl (12 M, 100 µl, 15.6 mmol) is added and the mixture is stirred at 80 °C for 3 h. The yellow precipitate obtained (product **14b**, 502 mg, 80%) is filtered and dried. ^{1}H NMR (300 MHz, $CDCl_3$) δ 8.37 – 8.24 (m, 3H), 7.90 (s, 2H), 7.51 (s, 1H).

*4.1.5 1-(4-(4-((5-chloro-4-((4-nitrophenyl)amino)pyrimidin-2-yl)amino)-3-methoxyphenyl)piperazin-1-yl)ethan-1-one (**16b**).* Compound **14b** (502 mg, 1.80 mmol) and aniline **15** (320 mg, 1.3 mmol) are suspended in *i*-PrOH (50 ml). PTSA*H_2O (1.92 mmol, 10.09 mmol) is added and the mixture is stirred at 80 °C for 15 h. The suspension is then cooled to room temperature and diluted with AcOEt, washed with $NaHCO_3$ and brine. The organic layer is dried over sodium sulfate and the solvents are removed under reduced pressure. The crude residue is purified by silica gel column chromatography (DCM/MeOH = 100:2) to afford the desired product as a yellow powder (0.40 gr, 45 %). ^{1}H NMR (300 MHz, $CDCl_3$) δ 8.26 – 8.17 (m, 2H), 8.15 (s, 1H), 7.98 (d, *J* = 8.6 Hz, 1H), 7.87 – 7.77 (m, 2H), 7.31 (d, *J* = 16.9 Hz, 2H), 6.60 – 6.47 (m, 2H), 3.89 (s, 3H), 3.87 – 3.76 (m, 2H), 3.71 – 3.62 (m, 2H), 3.19 – 3.11 (m, 4H), 2.16 (s, 3H).

*4.1.6 1-(4-(4-((4-((4-aminophenyl)amino)-5-chloropyrimidin-2-yl)amino)-3-methoxyphenyl)piperazin-1-yl)ethan-1-one (**17b**).* Compound **16a** (103 mg, 0.20 mmol) is dissolved in THF (15 ml). Zinc powder (126 mg, 2.17 mmol) and NH_4Cl 1M in water (0.5 ml, 0.5 mmol) are added and the mixture is heated at reflux for 2 h.

It is then cooled to room temperature and filtered on a pad of celite. The crude residue is purified by silica gel column chromatography (DCM/MeOH 10:0.5) to afford the desired aniline (40 mg, 43%). ^{1}H NMR (300 MHz, Chloroform-d) δ 8.11 (d, *J* = 8.8 Hz, 1H), 7.98 (s, 1H), 7.36 – 7.28 (m, 3H), 6.86 (s, 1H), 6.77 – 6.66 (m, 2H), 6.51 (d, *J* = 2.5 Hz, 1H), 6.42 (dd, *J* = 8.8, 2.5 Hz, 1H), 3.85 (s, 3H), 3.78 (t, *J* = 5.2 Hz, 2H), 3.65 – 3.53 (m, 2H), 3.22 – 3.02 (m, 4H), 2.14 (s, 3H).

*4.1.7 3-((2,5-dichloropyrimidin-4-yl)amino)benzoic acid (**14c**).* 2,4,5-trichloropyrimidine (619 mg, 3.37 mmol) and 3-amino benzoic acid (462 mg, 3.37 mmol) are suspended in water (20 ml). HCl (12 M, 100 µl, 1.2 mmol) is added and brought to reflux. The suspension is stirred at reflux for 2 h, then cooled to room temperature and the precipitate that is formed is recovered by suction filtration and washed with water. Compound **14c** (508 mg, 53%) is obtained as a white amorphous solid. ^{1}H NMR (400 MHz, DMSO-d_6) δ 9.69 (s, 1H), 8.41 (s, 1H), 8.18 (m, 1H), 7.87 (d, *J* = 10.4 Hz, 1H), 7.75 (d, *J* = 10.4 Hz, 1H), 7.52 (t, *J* = 10.4 Hz, 1H).

*4.1.8 3-((2-((4-(4-acetylpiperazin-1-yl)-2-methoxyphenyl)amino)-5-chloropyrimidin-4-yl)amino)benzoic (**16c**).* Compound **14c** (113 mg 0.40 mmol) and aniline **15** (99 mg, 0.40 mmol) are suspended in *i*-PrOH (3.5 ml). PTSA*H_2O (76 mg 0.40 mmol) is added and the mixture is stirred at 80 °C for 15 h. The suspension is then cooled to room temperature and diluted with AcOEt. The organic phase is washed with brine and dried over Na_2SO_4. After filtration and evaporation of the solvent, the crude material is purified by flash column chromatography (petroleum ether/ AcOEt 6:4 with increasing amounts of MeOH, 1% then 5% and finally 10%) to furnish **16c** (134 mg, 66%) as a brown amorphous solid. ^{1}H NMR (300 MHz, $CDCl_3$/CD_3OD) δ 8.13

(bs, 1H), 7.95 (s, 1H), 7.88 (d, *J* = 12.0, 1H), 7.83 (d, *J* = 10.8 Hz, 2H), 7.4 (t, *J* = 10.4 Hz, 1H), 6.53 (d, *J* = 3.2 Hz, 1H), 6.34 (dd, *J* = 8.7, 3.2 Hz, 1H), 3.84 (s, 3H), 3.73 (t, *J* = 5.2 Hz, 2H), 3.63 (t, *J* = 5.1 Hz, 2H), 3.09 (m, 4H), 2.13 (s, 3H).

*4.1.9 4-fluorophenyl 3-((2-((4-(4-acetylpiperazin-1-yl)-2-methoxyphenyl)amino)-5-chloropyrimidin-4-yl)amino)benzoate (**8**).*Compound **16c** (39 mg, 0.08 mmol) is dissolved in THF (2 ml). DIPEA (30 ml, 0.17 mmol) is added, followed by 4-fluoro phenol (30 mg, 0.27 mmol) and 1-etil-3 (3-dimetilaminopropil) carbodiimide (EDCI 15 mg, 0.1 mmol). The solution is stirred at room temperature for 18 h. The solvents are removed under reduced pressure and the crude material is subjected to flash column chromatography (Et_2O, with increasing amounts of MeOH, 3% and then 5%) to afford 8 (13 mg, 28%) as a white solid. Mp: 127 – 130 °C. ^{1}H NMR (400 MHz, $CDCl_3/CD_3OD$) δ 8.46 (t, *J* = 2.0 Hz), 8.01 (s, 1H), 7.99 (dt, *J* = 7.6, 1.2 Hz, 1H), 7.92 (d, *J* = 8.8 Hz), 7.87 (m, 1H), 7.54 (t, *J* = 8.0 Hz, 1H), 7.11 (m, 4H), 6.60 (d, *J* = 2.4 Hz, 1H), 6.30 (dd, *J* = 8.0, 2.4 Hz), 3.88 (s, 3H), 3.73 (t, *J* = 5.2 Hz, 2H), 3.63 (t, *J* = 5.2 Hz, 2H), 3.05 (m, 4H), 2.14 (s, 3H). ^{13}C NMR (100 MHz, $CDCl_3/CD_3OD$) δ 170.15, 165.19, 161.51, 159.09, 157.57, 156.56, 154.06, 149.46, 146.86, 138.80, 129.54, 128.87, 128.40, 125.74, 125.08, 123.11, 123.03, 122.49, 120.37, 115.85, 115.62, 108.36, 100.99, 55.29, 50.40, 50.07, 46.22, 41.46, 20.34. MS (ESI): *m/z*: calcd for $C_{30}H_{28}ClFN_6O_4$ $[M+H]^+$: 590.18; found: 590.87.

*4.1.10 N-(3-((2-((4-(4-Acetylpiperazin-1-yl)-2-methoxyphenyl)amino)-5-chloropyrimidin-4-yl)amino)phenyl)-2-chloroacetamide (**6**).* To a solution of chloroacetic acid (124 mg, 1.31 mmol) in anhydrous THF (2 ml) are added DIPEA (230 µl, 1.32 mmol) and pivaloyl chloride (140 µl, 1.13 mmol). After stirring at room temperature for 20 min,

a suspension of aniline **17a** (97 mg, 0.21 mmol) in anhydrous THF (3 ml) is added and the mixture is stirred for 1 h before being diluted with water. The mixture is extracted with AcOEt and the organic layer is washed with water and brine, dried over Na2SO4 and concentrated under reduced pressure. Purification of the solid residue by silica gel column chromatography (DCM + 3% MeOH) and crystallization from EtOH/water 7:3 afford the title compound **6** (61 mg, 54%) as colorless crystals. Mp: 172 °C. ^{1}H NMR (400 MHz, $CDCl_3/CD_3OD$) δ 7.94 (s, 1H), 7.94 (d, *J* = 11.8 Hz, 1H), 7.79 (t, *J* = 2.1 Hz, 1H), 7.42 (q, *J* = 2.1 Hz, 1H), 7.39 (t, *J* = 2.0 Hz, 1H), 7.32 (d, *J* = 7.9 Hz, 1H), 6.55 (d, *J* = 2.6 Hz, 1H), 6.37 (dd, *J* = 8.8, 2.5 Hz, 1H), 4.13 (s, 2H), 3.86 (s, 3H), 3.73 (t, *J* = 5.2 Hz, 2H), 3.66 (t, *J* = 5.2 Hz, 2H), 3.10 (dt, *J* = 14.1, 5.2 Hz, 4H), 2.13 (s, 3H); ^{13}C NMR (100 MHz, $CDCl_3/CD_3OD$) δ 170.00, 165.41, 157.59, 156.13, 153.86, 149.41, 146.79, 138.50, 137.79, 129.07, 122.73, 120.54, 119.12, 116.23, 114.36, 108.70, 104.38, 101.05, 55.55, 50.70, 50.38, 46.35, 42.91, 41.56, 20.85. MS (ESI): *m/z*: calcd for $C_{25}H_{28}Cl_2N_7O_3$ $[M+H]^+$: 544.16; found: 543.86.

4.1.11 N-(3-((2-((4-(4-acetylpiperazin-1-yl)-2-methoxyphenyl) amino)-5-chloropyrimidin-4-yl) amino) phenyl) ethene sulfonamide (7). A mixture of compound **17a** (90 mg, 0.19 mmol) and triethylamine (0.6 ml, 0.43 mmol) is dissolved in tetrahydrofuran (2 ml) and cooled with and ice-water bath. A solution of 2-bromoethane-1-sulfonyl chloride **19** (59 mg, 0.28 mmol) in tetrahydrofuran is added dropwise. The mixture is stirred under nitrogen for 24 h, then the solvent is removed. The crude product purified by silica gel column chromatography (toluene/acetone = 1:1) to afford **7** as a white solid (15 mg, 14%). Mp: 118 – 122 °C. ^{1}H NMR (400 MHz, $CDCl_3/CD_3OD$) δ

7.99 – 7.91 (m, 2H), 7.59 (d, *J* = 5.3 Hz, 1H), 7.35 – 7.07 (m, 5H), 7.01 – 6.95 (m, 1H), 6.65 – 6.54 (m, 2H), 6.49 (dd, *J* = 8.8, 2.5 Hz, 1H), 6.23 (d, *J* = 16.6 Hz, 1H), 5.92 (d, *J* = 9.9 Hz, 1H), 3.87 (s, 3H), 3.75 (t, *J* = 5.2 Hz, 2H), 3.68 (t, *J* = 5.1 Hz, 2H), 3.14 (dt, *J* = 22.4, 5.2 Hz, 4H), 2.15 (s, 3H). ^{13}C NMR (100 MHz, $CDCl_3$/CD_3OD) δ 170.13, 157.72, 156.23, 153.77, 149.66, 146.98, 139.06, 137.76, 135.50, 129.22, 127.27, 122.61, 120.84, 118.49, 115.86, 114.48, 108.74, 104.44, 101.12, 55.40, 50.63, 50.28, 46.32, 41.54, 20.62. MS (ESI): *m/z*: calcd for $C_{25}H_{28}ClN_7O_4S$ $[M+H]^+$: 558.17; found: 557.86.

*4.1.12 2-((3-((2-((4-(4-Acetylpiperazin-1-yl)-2-methoxyphenyl)amino)-5- chloropyrimidin-4-yl)amino)phenyl)amino)ethane-1-sulfonyl fluoride (**9**)*. Aniline **17a** (200 mg, 0.43 mmol) is dissolved in chloroform/MeOH 1:1 (10 ml) and ethenylsulfonyl fluoride (120 µl, 1.45 mmol) is added. The solution is stirred at room temperature for 3 h. TLC analysis reveals a conversion of about 40-50%. The mixture is diluted with AcOEt and washed with saturated aqueous $NaHCO_3$. The organic layer is consequently washed with water and brine, dried over Na_2SO_4 and concentrated under reduced pressure. Purification of the solid residue by silica gel column chromatography (toluene/EtOH 95:5) affords the title compound (33 mg, 13%) as a white solid. Mp: 89 °C. ^{1}H NMR (400 MHz, $CDCl_3$) δ 8.08 (d, *J* = 8.7 Hz, 1H), 8.05 (s, 1H), 7.23 – 7.16 (m, 2H), 7.00 (d, *J* = 2.0 Hz, 1H), 6.90 – 6.80 (m, 1H), 6.54 (d, *J* = 2.5 Hz, 1H), 6.48 (dd, *J* = 8.8, 2.6 Hz, 1H), 6.45 – 6.36 (m, 1H), 3.87 (s, 3H), 3.81 – 3.73 (m, 4H), 3.67 – 3.55 (m, 4H), 3.11 (dt, *J* = 12.5, 5.2 Hz, 4H), 2.15 (s, 3H). ^{13}C NMR (100 MHz, $CDCl_3$) δ 169.02, 155.57, 146.31, 139.41, 130.01, 120.91, 111.92, 108.71, 108.64, 106.34, 104.68, 101.09, 55.69, 50.82, 50.50, 49.95, 49.81, 46.30,

41.42, 38.19, 21.38. MS (ESI): *m/z*: calcd for $C_{25}H_{30}ClFN_7O_4$ $[M+H]^+$: 578.17; found: 577.90.

*4.1.13 3-((3-((2-((4-(4-acetylpiperazin-1-yl)-2-methoxyphenyl)amino)-5-chloropyrimidin-4-yl)amino)phenyl) carbamoyl) benzenesulfonyl fluoride (**10**).* A solution of aniline **17a** (50 mg, 0.1 mmol) in 2 ml of anhydrous tetrahydrofuran is added dropwise to a solution of 3-(fluorosulfonyl)benzoyl chloride **21** (0.5 mmol) in 1ml of pyridine placed at 0°C. The reaction is stirred at 0°C for 10min then the solvent is removed under reduced pressure. The crude residue is purified by silica gel column chromatography (toluene/acetone 7:3) to afford **10** as a white amorphous solid (14 mg, 21%). ^{1}H NMR (300 MHz, CD_3OD) δ 8.51 (t, *J* = 1.8 Hz, 1H), 8.32 (dt, *J* = 7.9, 1.4 Hz, 1H), 8.20 – 8.07 (m, 1H), 8.02 – 7.88 (m, 3H), 7.78 (t, *J* = 7.9 Hz, 1H), 7.59 – 7.49 (m, 1H), 7.34 – 7.29 (m, 2H), 7.20 – 6.99 (m, 2H), 3.81 (s, 3H), 3.54 (m, 4H), 2.91 (dt, J = 20.0, 5.2 Hz, 5H). MS (ESI): *m/z*: calcd for $C_{30}H_{29}ClFN_7O_5S$ $[M+H]^+$: 653.16; found: 653.86.

*4.1.14 4-(((4-((2-((4-(4-acetylpiperazin-1-yl)-2-methoxyphenyl)amino)-5-chloropyrimidin-4-yl)amino)phenyl) amino) methyl) benzenesulfonyl fluoride (**11**).* Compound **17b** (60 mg, 0.1 mmol), 4-(bromomethyl) benzenesulfonyl fluoride (35 mg, 0.13 mmol) and potassium carbonate (40 mg, 0.25 mmol) were dissolved in 3 ml of degassed DMF and stirred 2 hrs at 40°C. The reaction is cooled to room temperature and diluted with toluene and solvent removed under reduced pressure. The crude residue is purified by silica gel column chromatography (DCM/MeOH 10:0.2) to afford **11** as a white solid (30 mg, 35%). Mp: 188 – 192 °C. ^{1}H NMR (400 MHz, $CD_3OD/CDCl_3$) δ 8.12 (d, *J* = 8.8 Hz, 1H), 8.03 – 7.90 (m, 3H), 7.71 – 7.54 (m, 2H),

7.46 – 7.31 (m, 2H), 7.27 (s, 1H), 6.85 (s, 1H), 6.67 – 6.54 (m, 2H), 6.51 (d, *J* = 2.5 Hz, 1H), 6.41 (dd, *J* = 8.8, 2.5 Hz, 1H), 4.53 (s, 2H), 3.85 (s, 3H), 3.77 (t, *J* = 5.2 Hz, 2H), 3.67 – 3.57 (m, 2H), 3.07 (dt, *J* = 10.3, 5.2 Hz, 4H), 2.14 (s, 3H). ^{13}C NMR (101 MHz, $CD_3OD/CDCl_3$) δ 170.14, 157.60, 156.94, 152.82, 149.68, 149.19, 146.54, 145.48, 131.21, 130.96, 128.82, 128.54, 128.10, 127.92, 125.41, 123.04, 120.24, 112.74, 108.76, 104.08, 101.14, 55.41, 50.90, 50.32, 47.27, 46.32, 41.52, 20.61. MS (ESI): *m/z*: calcd for $C_{30}H_{31}ClFN_7O_4S$ $[M+H]^+$: 640.13; found: 640.10.

*4.1.15 N-(3-((2-((4-(4-Acetylpiperazin-1-yl)-2-methoxyphenyl)amino)-5-chloropyrimidin-4-yl)amino)phenyl)acetamide (**12**).* Aniline **17a** (49 mg, 0.11 mmol) is dissolved in pyridine (1 ml) and acetic anhydride (15 µl, 0.16 mmol) is slowly added. The mixture is stirred at room temperature for 30 min and diluted with water. The obtained precipitate is recovered by suction filtration and dried. Crystallization from water (10% MeOH added) affords the title compound (44 mg, 82%) as colorless, needle-like crystals. Mp: 168 °C. ^{1}H NMR (400 MHz, $CDCl_3/CD_3OD$) δ 7.96 (dd, *J* = 8.9, 1.3 Hz, 1H), 7.94 – 7.91 (m, 1H), 7.69 (s, 1H), 7.43 (dd, *J* = 7.6, 2.3 Hz, 1H), 7.36 – 7.30 (m, 1H), 7.27 (t, *J* = 8.0 Hz, 1H), 6.54 (d, *J* = 2.5 Hz, 1H), 6.45 – 6.31 (m, 1H), 3.85 (s, 3H), 3.73 (t, *J* = 5.2 Hz, 2H), 3.65 (t, *J* = 5.2 Hz, 2H), 3.09 (dt, *J* = 18.4, 5.3 Hz, 4H), 2.13 (s, 3H), 2.11 (d, *J* = 1.2 Hz, 3H). MS (ESI): *m/z*: calcd for $C_{25}H_{29}ClN_7O_3$ $[M+H]^+$: 510.19; found: 509.93.

4.2 Molecular Modelling

4.2.1 Docking. Docking simulations were performed with Glide 7.9 software [56] employing the crystal structure of the $EGFR^{L858R/T790M/V948R}$ where Lys745 is sulfonylated by XO44 and the kinase domain domain adopts an inactive

conformation (PDB code 5U8L) [36]. EGFR-XO44 covalent adduct was submitted to the protein preparation procedure implemented in Maestro 11.6 [57], which includes addition of hydrogen atoms and assignment of tautomeric state to His residues. The prepared EGFR-XO44 model was submitted to a geometric optimization in gas phase with OPLS3 force field [58], to a root mean square displacement (RMSD) value of 0.3 Å, to resolved unfavorable Van der Waals contacts. After optimization, XO44 was deleted from the active site and the atom type of the terminal nitrogen of Lys745 was conveniently modified. As recent investigations show that when the EGFR assumes an inactive conformation the basicity of this residue is depressed (estimated pKa = 7.3) [44], Lys745 was modeled in neutral form. The geometry of the model was further optimized by energy minimization (OPLS3 force field) in implicit water (GB/SA model) to an energy gradient of 0.01 kcal/(mol Å) and resulting structure employed for docking studies. The docking grid was centered on the centered of mass of the position occupied by XO44 in its covalent adduct with EGFR. Three-dimensional models of compounds **5**-**11** were built using Maestro and their geometries were optimized by energy minimization (OPLS3 with GB/SA model) to an energy gradient of 0.01 kcal/(mol ·Å). Docking simulations were performed starting from minimum energy conformations of compounds **5**-**11**, using a docking grid centered on Lys745. Enclosing and bounding boxes were set to 20 and 14 Å on each side, respectively. Van der Waals radii of the protein atoms were not scaled, while Van der Waals radii of the ligand atoms with partial atomic charges lower than |0.15| were scaled by 0.8. Standard precision (SP) mode was applied [59].

4.2.2 Covalent docking. Covalent docking simulations were performed using the covalent docking protocol [60] implemented in Glide 7.9 software, using the crystal structure of the $EGFR^{L858R/T790M/V948R}$, where Lys745 is sulfonylated by XO44 and the kinase domain adopts an inactive conformation (PDB code 5U8L). Following the same procedure applied in non-covalent docking simulations, the prepared protein structure was modified by removing the inhibitor and by modelling the Lys745 in its neutral form. The grid for covalent docking simulations was centered, for each ligand, on the position of the inhibitor in its non-covalent binding mode. Hydrogen-bonding constraints were applied, in order to retrieve docking poses in which the hinge-binding region moiety of the ligands takes polar contacts with the NH group of Met793 backbone. All the other parameters were set to their default values. 10 binding poses were collected for each ligand and ranked by their Prime energy. As the Prime energy is not suitable for comparing different ligands, the *cdock affinity score*, which measures the estimated affinity of the ligand to the protein for non-covalent binding prior to reaction, was calculated and used to compare the best Prime energy-ranked binding modes of **10** and **11**.

4.3 Pharmacology

4.3.1 Drug Treatments. Osimertinib was provided by AstraZeneca (Milan, Italy). Osimertinib and compounds were dissolved in DMSO (Sigma Aldrich, St Louis, MO, USA). Final concentration of DMSO in medium never exceeded 0.1% (v/v) and equal amounts of solvent were added to control cells.

4.3.2 Cell Culture. Ba/F3 cells harboring EGFR mutations ($EGFR^{del19/T790M/C797S}$ or $EGFR^{L858R/T790M/C797S}$) were kindly provided by Dr. Pasi Janne (Dana-Farber Cancer

Institute, Boston, MA, USA) and were cultured in RPMI-1640 growth medium, supplemented with 2 mM glutamine 10% fetal bovine serum (FBS, Invitrogen, Carlsbad, CA, USA) at 37°C in humidified 5% CO_2 incubator.

4.3.3 Western blot analysis. Cells were treated with compounds for 4h and then stimulated with 100 ng/ml EGF for 10 min. Procedures for protein extraction, solubilization, and protein analysis by 1-D PAGE are described elsewhere [8]. Antibodies against pEGFR(tyr1068), EGFR, actin, and HRP-conjugated secondary antibodies were from Cell Signaling Technology (Beverly, MA, USA); the chemiluminescence system (ImmobilionTM Western Chemiluminescent HRP Substrate) was from Millipore (Temecula, CA, USA). Reagents for electrophoresis and blotting analysis were from BIO-RAD (Hercules, CA, USA).

4.3.4 Cell viability assay. Cell viability assay was carried out by plating 20000 Ba/F3 cells per well into 96-well plates. On the same day the cells were treated with compounds and after 72h cell viability was measured using the MTS (methanethiosulfonate)-based assay (CellTiter 96® AQueous One Solution Cell Proliferation Assay; Promega, Madison, WI, USA). The cell viability was calculated as % of inhibition versus untreated control cells. All experiments were performed at least three times. Statistical analyses were carried out using GraphPad Prism version 6.0 software (GraphPad Software Inc., San Diego, CA, USA). Results are expressed as mean values ± standard deviations (SD).

4.3.5 Kinase activity assay. Invitrogen LanthaScreen® Eu Kinase Activity Assay, based on TR-FRET, was employed for both inhibitory potency (IC_{50}) determination and rapid dilution assays (Thermo Fisher Scientific, USA). For kinase activity assays, 0.89 nM

recombinant GST-EGFR (*WT,* Part Number PV3872) or 0.38 nM of GST-EGFR$^{L858R/T790M/C797S}$ (*TM*, Part Number A33502) or 5.62 nM of GST-EGFR$^{del19/T790M/C797S}$ (*DEL*, by Promega Italia S.r.l., Part Number VA7105), 100 (for *WT*) or 200 nM (for *TM* and *DEL*) Alexa Fluor 647-Poly-GT (peptide substrate, Part Number PV5693) and 2.5 (for *WT* and *DEL*) or 9 μM (for *TM*) ATP (Part Number PV3227) were incubated in Kinase Buffer A (50 mM HEPES pH 7.5, 10 mM $MgCl_2$, 1 mM EGTA, 0.01% Brij-35) in the absence or in the presence of different concentrations of EGFR inhibitors (range:10 μM-40 pM) for 1 h at room temperature in a black, low-volume 384-well plate (Corning Inc., USA) to allow substrate phosphorylation. For pre-incubation experiments, gefitinib (**1**), osimertinib (**4**) and compounds **9-12** were pre-incubated for 3 h with the recombinant GST-kinase before addition of peptide substrate and ATP mixture. For pre-incubation experiments in the presence of ATP, **11** was co-incubated with the recombinant GST-EGFR$^{L858R/T790M/C797S}$ and with ATP at a concentration equal to its K_m or 10-fold higher (9 μM and 90 μM of ATP, respectively) for 3h, then peptide and a fresh aliquot of 9 μM ATP were added. After incubation with the substrate, the plate was added with a solution of 2 nM Eu-PY20 antibody (Part Number PV5692) and Kinase Quench Buffer (EDTA solution, Part Number P2825, at a final concentration of 10 mM) in TR-FRET Dilution Buffer (Part Number PV5692) to stop reaction and incubated again for 30 min at room temperature to allow complexation of phosphorylated peptide and Eu-PY20 antibody. Then emission was recorded at *i.* 665 nm corresponding to the binary complex formation between phosphorylated substrate and Eu-PY20 antibody and at *ii.* 620 nm corresponding to Eu-PY20 antibody

intrinsic emission. The 665/620 emission ratio was plotted against molar concentrations of the inhibitor (on a log scale) to obtain the inhibitor concentration-kinase activity curve and calculate IC_{50} values. A Tecan Spark 10M plate reader (Tecan Italia Srl, Italy) was employed for data acquisition. Instrument settings were as follows: excitation filter: 340 nm (35 nm bandpass); emission filters: 665 nm (5 nm bandpass); 620 nm (10 nm bandpass); delay time: 100 μs; integration time: 200 μs; gain: optimal. Reported are mean values together with their standard error of the mean (n = 3-5). GraphPad Prism 5.03 (GraphPad Inc, USA) was employed for nonlinear fitting of experimental data to get final IC_{50} values.

4.3.6 Rapid dilution assay. For rapid dilution assays, LanthaScreen® Eu Kinase Activity Assay procedure was optimized as follows. Recombinant GST-$EGFR^{WT}$ or GST-$EGFR^{L858R/T790M/C797}$ was incubated at 100-fold the operative concentration used in kinase activity assays together with a concentration of gefitinib (**1**), osimertinib (**4**), XO44 and compounds **10-12** equal to 10-fold the respective IC_{50} value obtained in the 3 h-pre-incubation activity assay. After 3 h pre-incubation, the mixture was diluted 100-fold in Kinase Buffer A containing Alexa Fluor 647-Poly-GT and ATP at the operative concentrations reported above. 30 min after dilution, a solution of 2 nM Eu-PY20 antibody and Kinase Quench Buffer in TR-FRET Dilution Buffer was added to the plate that was incubated again for 30 min at room temperature before TR-FRET detection. Follow-up analyses were conducted using Student's t-test. Statistical significance was set at $p < 0.05$.

4.3.7 Selectivity Assay. Inhibitory activity for selected compounds (XO44, **11** and **12**) was measured at 0.1 (XO44, **11**) and 1 μM (XO44, **11**, **12**) in a set of serine-threonine

kinases (AKT-2, AMP-K, aurora kinase A, CDK-2, CDK-5, ERK1, IKKβ, p38α, ROCK-1) and tyrosine kinases (BLK, LCK, SRC, FGFR-4, JAK1, PDGFRα, VEGR2). The kinase activity of each enzyme was measured in the presence of an ATP concentration equal to the K_m value, detecting the FRET signal generated by the kinase-catalyzed phosphorylation of a reference peptide. (Z'-LYTE assay, Thermo Fisher Scientific, Madison, WI, USA). Compounds were tested in 1% DMSO solution.

4.4 Investigation of covalent modification of EGFR$^{L858R/T790M/C797S}$ by LC-HRMS

4.4.1 Sample preparation. Recombinant EGFR$^{L858R/T790M/C797S}$ and **11** or control vehicle (DMSO) were co-incubated at 1:5 molar ratio for 1 h in Kinase Buffer A. The two samples underwent the following reduction/alkylation/digestion protocol. Samples were added with 5 µL of 50 mM ammonium bicarbonate buffer solution pH 8.0 (ABC) and 2 µL of a 500 mM solution of dithiothreitol in 50 mM ABC, for 15 min at 60°C; then cysteine alkylation occurred by addition of 2 µL of a 1 M solution of iodoacetamide in ABC buffer for 15 min at room temperature in the dark. Trypsin digestion took place overnight at 37 °C using 0.1 µg of trypsin per sample (trypsin:recombinant EGFR ratio equal to 1:10). Reaction was stopped by adding 2 µL of a 20% v/v formic acid solution. Digested samples were then subjected to purification and concentration using ZipTip with C_{18} resin (Millipore, Part Number ZTC18S096), eluting peptides in 50%ACN in water added with 0.1% formic acid. The eluate was analysed *via* LC-HRMS.

4.4.2 Mass spectrometry analysis. LC-HRMS analyses were performed on a Thermo LTQ-Orbitrap mass spectrometer (Thermo Fisher Scientific) interfaced to a Dionex

Ultimate 3000 HPLC system (Thermo Fisher Scientific) by mean of an electrospray ionization (ESI) source. Chromatographic separation was achieved on a Phenomenex Synergy Fusion 80 Å column (2.1×100 mm, i.d., 4 μm) with mobile phase consisting of water (A) and acetonitrile (B), both added with 0.2% formic acid. The following gradient was used for elution: 0–5 min 2% B, 5–64 min 2–60% B, 64–65 min 60-90% B, 65-70 min 90% B, 70-71 min 90-2% B; 71-80 min 90%B, with a flow rate of 0.30 ml/min. ESI source was operated in positive ion mode (ESI^+) with the source parameters optimized as follows: capillary voltage: 3 kV; capillary temperature: 275 °C; sheath gas (nitrogen gas) flow rate: 40 arbitrary units; auxiliary gas (nitrogen gas): flow rate 10 arbitrary units. The data were acquired in the mass range of *m/z* 200–1000 amu with resolution of 100,000 FWHM. MS/MS spectra of the peptides were obtained in Collision Induced Dissociation (CID) mode, setting the collision energy at 35 V. Xcalibur software (Version 2.3.1, Thermo Fisher Scientific, USA) was used for both data acquisition and processing. Proteome Discoverer software (Version 2.3.0.523, Thermo Fisher Scientific, USA) was employed for peptide mass fingerprint and covalent modification analysis.

FUNDING

This work was supported by Associazione Italiana per la Ricerca sul Cancro (AIRC), Milan Grant IG2017-20074 (PI Marcello Tiseo).

DECLARATION OF COMPETING INTEREST

The authors declare that they have no known competing financial interests or personal relationships that could have appeared to influence the work reported in this paper.

ACKNOWLEDGMENT

The authors are grateful to the Centro Interdipartimentale Misure "Giuseppe Casnati" of the University of Parma for providing NMR instrumentation, and to Dr. Pasi Janne (Dana-Farber Cancer Institute, Boston, MA, USA) to provide Ba/F3 cells harboring $EGFR^{del19/T790M/C797S}$ or $EGFR^{L858R/T790M/C797S}$ mutation.

APPENDIX A. SUPPLEMENTARY DATA

Supplementary data to this article can be found online

REFERENCES

[1] Roskoski, R. Jr. The ErbB/HER family of protein-tyrosine kinases and cancer. *Pharmacol. Res.* **2014**, *79*, 34-74.

[2] Niggenaber, J.; Hardick, J.; Lategahn, J.; Rauh, D. Structure defines function: clinically relevant mutations in ErbB kinases. *J. Med. Chem.* **2020**, *63*, 40-51.

[3] Okabe, T.; Okamoto, I.; Tamura, K.; Terashima, M.; Yoshida, T.; Satoh T, Takada, M.; Fukuoka, M.; Nakagawa, K. Differential constitutive activation of the epidermal growth factor receptor in non-small cell lung cancer cells bearing EGFR gene mutation and amplification. *Cancer Res.* **2007**, *67*, 2046-2053.

[4] Paez, J.G.; Jänne, P. A.; Lee, J. C.; Tracy, S.; Greulich, H.; Gabriel, S.; Herman, P.; Kaye, F. J.;Lindeman, N.; Boggon, T. J.; Naoki, K.; Sasaki, H.; Fujii, Y.; Eck, M. J.; Sellers, W. R.; Johnson, B. E.; Meyerson, M. EGFR Mutations in lung cancer: correlation with clinical response to gefitinib therapy. *Science* **2004**, *304*, 1497-1500.

[5] Engelman, J. A.; Janne, P. A. Mechanisms of acquired resistance to epidermal growth factor receptor tyrosine kinase inhibitors in non-small cell lung cancer. *Clin. Cancer Res.* **2008**, *14*, 2895-2899.

[6] Kobayashi, S.; Boggon, T. J.; Dayaram,T.;Jañne, P. A.; Kocher, O.; Meyerson, M.; Johnson, B. E.; Eck, M. J.; Tenen, D. G.; Halmos, B. EGFR mutation and resistance of non-small-cell lung cancer to gefitinib. *N. Engl. J. Med.* **2005**, 352, 786-792.

[7] Yun, C.-H.; Mengwasser, K. E.; Toms, A. V.; Woo, M. S.; Greulich, H.; Wong, K.-K.; Meyerson, M.; Eck, M. J. The T790M Mutation in EGFR kinase causes drug resistance by increasing the affinity for ATP. *Proc. Natl. Acad. Sci. U.S.A.* **2008**, *105*, 2070-2075.

[8] a) Carmi, C.; Cavazzoni, A.; Vezzosi, S.; Bordi, F.; Vacondio, F.; Silva, C.; Rivara, S.; Lodola, A.; Alfieri, R. R.; La Monica, S.; Galetti, M.; Ardizzoni, A.; Petronini, P. G.; Mor, M. Novel irreversible epidermal growth factor receptor inhibitors by chemical modulation of the cysteine-trap portion. *J. Med. Chem.* **2010**, *53*, 2038-2050; b) Castelli, R.; Bozza, N.; Cavazzoni, A.; Bonelli, M.; Vacondio, F.; Ferlenghi, F.; Callegari, D.; Silva, C.; Rivara, S.; Lodola, A.; Digiacomo, G.; Fumarola, C.; Alfieri, R.; Petronini, P. G, Mor, M. Balancing reactivity and antitumor activity: heteroarylthioacetamide derivatives as potent and time-dependent inhibitors of EGFR. *Eur. J. Med. Chem.* **2019***, 162*, 507-524.

[9] a) Hirsh, V. Afatinib (BIBW 2992) Development in non-small-cell lung cancer. *Future Oncol.* **2011**, *7*, 817-825. b) Lau, S. C. M.; Batra, U.; Mok, T. S. K.; Loong, H. H. Dacomitinib in the management of advanced non-small-cell lung cancer. *Drugs* **2019**, *79*, 823-831.

[10] Cheng, H.; Nair, S. K.; Murray, B.W. Recent progress on third generation covalent EGFR inhibitors. *Bioorg. Med. Chem. Lett.* **2016**, *26*, 1861-1868.

[11] Zhou, W.; Ercan, D.; Chen, L.; Yun, C.-H.; Li, D.; Capelletti, M.; Cortot, A. B.; Chirieac, L.; Iacob, R. E.; Padera, R.; Engen, J. R.; Wong, K.-K.; Eck, M. J.; Gray, N. S.; Jänne, P. A. Novel mutant-selective EGFR kinase inhibitors against EGFR T790M. *Nature* **2009**, *462*, 1070-1074.

[12] Sequist, L. V., Soria, J. C., Goldman, J. W.; Wakelee, H. A.; Gadgeel, S. M.; Varga, A.; Papadimitrakopoulou, V.; Solomon, B. J.; Oxnard, G. R.; Dziadziuszko, R.; Aisner, D. L.; Doebele R. C.; Galasso, C.; Garon, E. B.; Heist, R. S.; Logan, J.; Neal, J. W.; Mendenhall, M. A.; Nichols, S.; Piotrowska, Z.; Wozniak, A. J.; Raponi, M.; Karlovich, C. A.; Jaw-Tsai, S.; Isaacson, J.; Despain, D.; Matheny, S. L.; Rolfe, L.; Allen, A. R.; Camidge, D. R. Rociletinib in EGFR-mutated non-small-cell lung cancer. *N. Engl. J. Med.* **2015**, *372*, 1700-1709.

[13] a) Finlay, M. R. V.; Anderton, M.; Ashton, S.; Ballard, P.; Bethel, P. A.; Box, M. R.; Bradbury, R. H.; Brown, S. J.; Butterworth, S.; Campbell, A.; Chorley, C.; Colclough, N.; Cross, D. A. E.; Currie, G. S.; Grist, M.; Hassall, L.; Hill, G. B.; James, D.; James, M.; Kemmitt, P.; Klinowska, T.; Lamont, G.; Lamont, S. G.; Martin, N.; McFarland, H. L.; Mellor, M. J.; Orme, J. P.; Perkins, D.; Perkins, P.; Richmond, G.; Smith, P.; Ward, R. A.; Waring, M. J.; Whittaker, D.; Wells, S.; Wrigley, G. L. Discovery of a potent and selective EGFR inhibitor (AZD9291) of both sensitizing and T790M resistance mutations that spares the wild type form of the receptor. *J.*

Med. Chem. **2014**, *57*, 8249-8267. b) Cross, D. A. E.; Ashton, S. E.; Ghiorghiu, S.; Eberlein, C.; Nebhan, C. A.; Spitzler, P. J.; Orme, J. P.; Finlay, M. R. V.; Ward, R. A.; Mellor, M. J.; Hughes, G.; Rahi, A.; Jacobs, V. N.; Brewer, M. R.; Ichihara, E.; Sun, J.; Jin, H.; Ballard, P.; Al-Kadhimi, K.; Rowlinson, R.; Klinowska, T.; Richmond, G. H. P.; Cantarini, M.; Kim, D.-W.; Ranson, M. R.; Pao, W. AZD9291, an irreversible EGFR TKI, overcomes T790M-mediated resistance to EGFR inhibitors in lung cancer. *Cancer Discovery* **2014**, *4*, 1046-1061.

[14] Song, Z.; Ge, Y.; Wang, C.; Huang, S.; Shu, X.; Liu, K.; Zhou, Y.; Ma, X. Challenges and Perspectives on the Development of Small-Molecule EGFR Inhibitors against T790M-Mediated Resistance in Non-Small- Cell Lung Cancer. *J. Med. Chem.* **2016**, *59*, 6580-6594.

[15] Dolly, S. O.; Collins, D. C.; Sundar, R.; Popat, S.; Yap, T. A. Advances in the development of molecularly targeted agents in non- small-cell lung cancer. *Drugs* **2017**, *77*, 813-827.

[16] Ramalingam, S. S.; Vansteenkiste, J.; Planchard, D.; Cho, B. C.; Gray, J. E.; Ohe, Y.; Zhou C.; Reungwetwattana, T.; Cheng, Y.; Chewaskulyong, B.; Shah, R.; Cobo, M.; Lee, K. H.; Cheema, P.; Tiseo, M.; John, T.; Lin, M. C.; Imamura, F.; Kurata, T.; Todd, A.; Hodge, R.; Saggese, M.; Rukazenkov, Y.; Soria, J. C; FLAURA Investigators. Overall survival with osimertinib in untreated, EGFR-mutated advanced NSCLC. *N. Engl. J. Med.* **2020,** *382*, 41-50.

[17] a) Leonetti, A.; Sharma, S.; Minari, R.; Perego, P.; Giovannetti, E.; Tiseo, M. Resistance mechanisms to osimertinib in EGFR-mutated non-small cell lung cancer. *Br. J. Cancer.* **2019**, 121, 725-737; b) Tumbrink, H. L.; Heimsoeth, A.; Sos, M. L. The next tier of EGFR resistance mutations in lung cancer. *Oncogene* **2021,** *40*, 1-11.

[18] Lee J, Kim HS, Lee B, Kim HK, Sun JM, Ahn JS, Ahn MJ, Park K, Lee SH. Genomic landscape of acquired resistance to third-generation EGFR tyrosine kinase inhibitors in EGFR T790M-mutant non-small cell lung cancer. *Cancer* **2020**, *126*, 2704-2712.

[19] Thress, K. S; Paweletz, C. P; Felip, E.; Cho, B. C.; Stetson, D.; Dougherty, B.; Lai, Z.; Markovets, A.; Vivancos, A.; Kuang, Y.; Ercan, D.; Matthews, S. E; Cantarini, M.; Barrett, J C.; Janne, P. A; Oxnard, G. R. Acquired EGFR C797S mutation mediates resistance to AZD9291 in non-small cell lung cancer harboring EGFR T790M. *Nat. Med.* **2015**, *21*, 560-562.

[20] He, J.; Zhou, Z.; Sun, X.; Yang, Z.; Zheng, P.; Xu, S.; Zhu, W. The new opportunities in medicinal chemistry of fourth-generation EGFR inhibitors to overcome C797S mutation. *Eur. J. Med. Chem.* **2021**; *210*, 112995.

[21] Heppner, D. E.; Günther, M.; Wittlinger, F.; Laufer, S. A.; Eck, M. J. Structural basis for EGFR mutant inhibition by trisubstituted imidazole inhibitors. *J. Med. Chem.* **2020**, *63*, 4293-4305.

[22] Günther, M.; Lategahn, J.; Juchum, M.; Döring, E.; Keul, M.; Engel, J.; Tumbrink, H. L.; Rauh, D.; Laufer, S. Trisubstituted pyridinylimidazoles as potent inhibitors of the clinically resistant L858R/T790M/C797S EGFR mutant: targeting of both hydrophobic regions and the phosphate binding site. *J. Med. Chem.* **2017**, *60*, 5613-5637.

[23] Lu, X.; Zhang, T.; Zhu, S.-J.; Xun, Q.; Tong, L.; Hu, X.; Li, Y.; Chan, S.; Su, Y.; Sun, Y.; Chen, Y.; Ding, J.; Yun, C.-H.; Xie, H.; Ding, K. Discovery of JND3229 as a new EGFR C797S mutant inhibitor with in vivo monodrug efficacy. *ACS Med. Chem. Lett.* **2018**, *9*, 1123-1127.

[24] Kashima, K.; Kawauchi, H.; Tanimura, H.; Tachibana, Y.; Chiba, T.; Torizawa, T.; Sakamoto H. CH7233163 overcomes osimertinib resistant EGFR-Del19/T790M/C797S mutation. *Mol. Cancer Ther.* **2020**, *11*, 2288-2297.

[25] Engelhardt, H.; Böse, D.; Petronczki, M.; Scharn, D.; Bader, G.; Baum, A.; Bergner, A.; Chong, E.; Döbel, S.; Egger, G.; Engelhardt, C.; Ettmayer, P.; Fuchs, J. E.; Gerstberger, T.; Gonnella, N.; Grimm, A.; Grondal, E.; Haddad, N.; Hopfgartner, B.; Kousek, R.; Krawiec, M.; Kriz, M.; Lamarre, L.; Leung, J.; Mayer, M.; Patel, N. D.; Simov, B. P.; Reeves, J. T.; Schnitzer, R.; Schrenk, A.; Sharps, B.; Solca, F.; Stadtmüller, H.; Tan, Z.; Wunberg, T.; Zoephel, A.; McConnell, D. B. Start selective and rigidify: the discovery path toward a next generation of EGFR tyrosine kinase inhibitors. *J. Med. Chem.* **2019**, *62*, 10272-10293.

[26] Palmieri, L.; Rastelli, G. αC helix displacement as a general approach for allosteric modulation of protein kinases. *Drug Discov. Today* **2013**, *18*, 407-414.

[27] To, C.; Jang, J.; Chen, T.; Park, E.; Mushajiang, M.; De Clercq, D. J. H.; Xu, M.; Wang, S.; Cameron, M. D.; Heppner, D. E.; Shin, B. H.; Gero, T. W.; Yang, A.; Dahlberg, S. E.; Wong, K.-K.; Eck, M. J.; Gray, N. S.; Janne, P. A. Single and dual targeting of mutant EGFR with an allosteric inhibitor. *Cancer Discovery* **2019**, *9*, 926-943.

[28] Grabe, T.; Lategahn, J.; Rauh, D. C797S resistance: the undruggable EGFR mutation in non-small cell lung cancer? *ACS Med. Chem. Lett.* **2018**, *9*, 779-782.

[29] Abdeldayem, A.; Raouf Y. S.; Constantinescu, S. N, Moriggl, R.; Gunning, P. T. Advances in covalent kinase inhibitors. *Chem. Soc. Rev.* **2020**, *49*, 2617-2687.

[30] Cuesta, A.; Taunton, J. Lysine-targeted inhibitors and chemoproteomic probes. *Annu. Rev. Biochem.* **2019**, *88*, 365-381.

[31] Lonsdale, R.; Ward, R. A. Structure-based design of targeted covalent inhibitors. *Chem. Soc. Rev.* **2018**, *47*, 3816-3830.

[32] a) Capoferri, L.; Lodola, A.; Rivara, S.; Mor, M. Quantum mechanics/molecular mechanics modeling of covalent addition between EGFR-cysteine 797 and N-(4-anilinoquinazolin-6-yl) acrylamide. *J. Chem. Inf. Model.* **2015**, *55*, 589-599. b) Lodola, A.; Callegari, D.; Scalvini, L.; Rivara, S.; Mor M. Design and SAR analysis of covalent inhibitors driven by hybrid QM/MM simulations. *Methods Mol. Biol.* **2020**, *2114*, 307-337.

[33] Jura, N.; Zhang, X.; Endres, N. F.; Seeliger, M. A.; Schindler, T.; Kuriyan, J. Catalytic control in the EGF receptor and its connection to general kinase regulatory mechanisms. *Mol Cell.* **2011** *42*, 9-22.

[34] Gehringer, M.; Laufer, S. A. Emerging and re-emerging warheads for targeted covalent inhibitors: applications in medicinal chemistry and chemical biology. *J. Med. Chem.* **2019**, *62*, 5673-5724.

[35] Pettinger, J.; Jones, K.; Cheeseman, M. D. Lysine-targeting covalent inhibitors. *Angew. Chem. Int. Ed. Engl.* **2017**, *56*, 15200-15209.

[36] Zhao, Q.; Ouyang, X.; Wan, X.; Gajiwala, K. S.; Kath, J. C.; Jones, L. H.; Burlingame, A. L.; Taunton, J. Broad-spectrum kinase profiling in live cells with lysine-targeted sulfonyl fluoride probes. *J. Am. Chem. Soc.* **2017**, *139*, 680-685.

[37] Statsuk, A. V.; Maly, D. J.; Seeliger, M. A.; Fabian, M. A.; Biggs, W. H. 3rd; Lockhart, D. J.; Zarrinkar, P. P.; Kuriyan, J.; Shokat, K. M. Tuning a three-component reaction for trapping kinase substrate complexes. *J. Am. Chem .Soc.* **2008**, *130*, 17568-17574.

[38] Gushwa, N. N.; Kang, S.; Chen, J.; Taunton, J. Selective targeting of distinct active site nucleophiles by irreversible SRC-family kinase inhibitors. *J Am Chem Soc.* **2012**, *134*, 20214-20207.

[39] Jones, L. H.; Kelly, J. W. Structure-based design and analysis of SuFEx chemical probes. *RSC Med. Chem.* **2020**, 11, 10-17.

[40] Zhai, X.; Ward, R. A.; Doig, P.; Argyrou, A. Insight into the therapeutic selectivity of the irreversible EGFR tyrosine kinase inhibitor osimertinib through enzyme kinetic studies. *Biochemistry* **2020**, *59*, 1428-1441.

[41] Anscombe, E.; Meschini, E.; Mora-Vidal, R.; Martin, M. P.; Staunton, D.; Geitmann, M.; Danielson, U. H.; Stanley, W. A.; Wang, L. Z.; Reuillon, T.; Golding, B. T.; Cano, C.; Newell, D. R.; Noble, M. E.; Wedge, S. R.; Endicott, J. A.; Griffin, R. J. Identification and characterization of an irreversible inhibitor of CDK2. *Chem. Biol.* **2015**, *22*, 1-6.

[42] Dalton, S. E.; Dittus, L.; Thomas, D. A.; Convery, M. A.; Nunes, J.; Bush, J. T.; Evans, J. P.; Werner, T.; Bantscheff, M.; Murphy, J. A.; Campos, S. Selectively targeting the kinome conserved lysine of PI3Kδ as a general approach to covalent kinase inhibition. *J. Am. Chem. Soc.* **2018**, *140*, 932-939.

[43] Mukherjee, H.; Debreczeni, J.; Breed, J.; Tentarelli, S.; Aquila, B.; Dowling, J. E.; Whitty, A.; Grimster, N. P. A study of the reactivity of S(VI)-F containing warheads with nucleophilic amino-acid side chains under physiological conditions. *Org Biomol Chem.* **2017**, *15*, 9685-9695.

[44] Liu, R.; Yue, Z.; Tsai, C. C.; Shen, J. Assessing lysine and cysteine reactivities for designing targeted covalent kinase inhibitors. *J. Am. Chem. Soc.* **2019**, *141*, 6553-6560.

[45] Yan, X. E.; Zhu, S. J.; Liang, L.; Zhao, P.; Choi, H. G.; Yun, C. H. Structural basis of mutant-selectivity and drug-resistance related to CO-1686. *Oncotarget* **2017**, *8*, 53508-53517.

[46] Yan, X. E.; Ayaz, P.; Zhu, S. J.; Zhao, P.; Liang, L.; Zhang, C. H.; Wu, Y. C.; Li, J. L.; Choi, H. G.; Huang, X.; Shan, Y.; Shaw, D. E.; Yun, C. H. Structural basis of AZD9291 selectivity for EGFR T790M. *J. Med. Chem.* **2020**, *63*, 8502-8511.

[47] Ward, R. A.; Anderton, M. J.; Ashton, S.; Bethel, P. A.; Box, M.; Butterworth, S.; Colclough, N.; Chorley, C. G.; Chuaqui, C.; Cross, D. A. E.; Dakin, L. A.; Debreczeni, J. É.; Eberlein, C.; Raymond, M.; Finlay, V.; Hill, G. B.; Grist, M.; Klinowska, T. C. M.; Lane, C.; Martin, S.; Orme, J. P.; Smith, P.; Wang, F.; Waring M. J. Structure- and Reactivity-Based Development of Covalent Inhibitors of the Activating and Gatekeeper Mutant Forms of the Epidermal Growth Factor Receptor (EGFR). *J. Med. Chem.* **2013**, *56*, 7025-7048.

[48] Marvel, C. S.; Bailey, C. F.; Sparberg, M. S. A synthesis of Taurine. *J. Am. Chem. Soc.* **1927**, *49*, 1833-1837.

[49] Kreimeyer, A.; Laube, B.; Sturgess, M.; Goeldner, M.; Foucaud, B. Evaluation and biological properties of reactive ligands for the mapping of the glycine site on the *N*-methyl-D-aspartate (NMDA) receptor. *J. Med. Chem.* **1999**, *42*, 4394-4404.

[50] Grimster, N. P.; Connelly, S.; Aleksandra Baranczak, A.; Dong, J.; Larissa B. Krasnova, L. B.; Sharpless, K. B.; Evan T. Powers, E. T.; Ian A. Wilson, I. A.;. Kelly, J. W. Aromatic sulfonyl fluorides covalently kinetically stabilize transthyretin to prevent amyloidogenesis while affording a fluorescent conjugate. *J. Am. Chem. Soc.* **2013**, *135*, 5656-5668.

[51] Briana J. Davie B. J.; Celine Valant, C.; White,, J. M.; Sexton, P. M.; Capuano, B.; Christopoulos, A.; Scammells, P. J. Synthesis and pharmacological evaluation of analogues of benzyl quinolone carboxylic acid (BQCA) designed to bind irreversibly to an allosteric site of the M1 muscarinic acetylcholine receptor. *J. Med. Chem.* **2014**, *57*, 5405-5418.

[52] Thorarensen, A.; Balbo, P.; Banker, M. E.; Czerwinski, R. M.; Kuhn, M.; Maurer, T. S. Telliez J. B.; Vincent, F.; Wittwer, A. J. The advantages of describing covalent inhibitor in vitro potencies by IC50 at a fixed time point. IC50 determination of covalent inhibitors provides meaningful data to medicinal chemistry for SAR optimization. *Bioorg Med Chem*. **2021,** *29*, 115865.

[53] Barf, T.; Kaptein, A. Irreversible protein kinase inhibitors: balancing the benefits and risks. *J. Med. Chem*. **2012**, *55*, 6243-6262.

[54] Uchibori, K.; Inase, N.; Araki, M.; Kamada, M.; Sato, S.; Okuno, Y.; Fujita, N.; Katayama, R. Brigatinib combined with anti-EGFR antibody overcomes osimertinib resistance in EGFR mutated non-small-cell lung cancer. *Nat. Commun.* **2017**, *8*, 14768.

[55] Perona JJ, Craik CS. Evolutionary divergence of substrate specificity within the chymotrypsin-like serine protease fold. *J Biol. Chem.* **1997**, *272*, 29987-29990.

[56] Glide, Schrödinger, LLC, New York, NY, 2019.

[57] Maestro, Schrödinger, LLC, New York, NY, 2019.

[58] Harder, E.; Damm, W.; Maple, J.; Wu, C.; Reboul, M.; Xiang, J. Y.; Wang, L.; Lupyan, D.; Dahlgren, M. K.; Knight, J. L.; Kaus, J. W.; Cerutti, D. S, Krilov, G.; Jorgensen, W. L.; Abel, R.; Friesner, R. A. OPLS3: a force field providing broad coverage of druglike small molecules and proteins. *J. Chem. Theory Comput.* **2016**, *12*, 281-296.

[59] Friesner, R. A.; Banks, J. L.; Murphy, R. B.; Halgren, T. A.; Klicic, J. J.; Mainz, D. T.; Repasky, M. P.; Knoll, E. H.; Shaw, D. E.; Shelley, M.; Perry, J. K.; Francis, P.; Shenkin, P. S., Glide: A New Approach for Rapid, Accurate Docking and Scoring. 1. Method and Assessment of Docking Accuracy. *J. Med. Chem.* **2004**, *47*, 1739-1749.

[59] Zhu, K.; Borrelli, K. W.; Greenwood, J. R.; Day, T. ; Abel, R.; Farid, R. S.; Harder, E. Docking covalent inhibitors: A parameter free approach to pose prediction and scoring, *J. Chem. Inf. Model.* **2014**, *54*, 1932−1940.

Graphical Abstract